Journal of Structural Dynamics

An Efficient Method for Calculating Hysteretic Dry Friction Response of Dynamic Systems Subjected to Combined Harmonic and Random Excitation

John Hickey *[1] and Tore Butlin †[2]

[1] *Department of Civil, Structural & Environmental Engineering, Trinity College Dublin, College Green, Dublin 2, Ireland*
[2] *Department of Engineering, University of Cambridge, Trumpington Street, Cambridge, United Kingdom*

Abstract

Many examples of dynamic analysis require modelling of dry friction. Often this is represented by a so-called Jenkins element or multiple Jenkins elements in parallel, which is sometimes termed a parallel-series Iwan element. This study considers the case where a system that includes these representations of dry friction are loaded dynamically with a combination of deterministic harmonic and random excitation. This paper presents a new efficient method for predicting the response of systems subject to combined deterministic and random excitation. The method is based on equivalent linearisation and involves averaging across both an ensemble of random responses as well as over a harmonic excitation period. The key novelty in the approach is the use of an auxiliary harmonic term to facilitate an analytical representation of the nonlinear force. This overcomes the challenge of analysing a discontinuous hysteretic nonlinearity in the presence of random excitation. Analytical solutions are presented and it is shown that the proposed approach can predict the approximate response at a significantly reduced computational cost.

Keywords: Nonlinear dynamics; Friction; Hysteretic Nonlinearity; Equivalent Linearization; Combined Excitation

Received on March 30, 2024, *Accepted on July 29, 2024*, *Published on September 8, 2024*

1 Introduction

Modelling friction at contact interfaces is often necessary in structural dynamics [1]. It has been estimated that up to 90% of total energy dissipation may be provided by joints of an assembled structure [2], indicating that the influence of frictional joints and interfaces on dynamic response can be substantial [3].

It is common to represent dry friction using a so-called Jenkins element [4]. Sometimes termed a Prandtl element [5], the elastic Coulomb or elastic sliding model, it is a relatively simple way to model dry friction, combining a Coulomb friction slider with an elastic spring to produce a piecewise linear force-displacement relationship. Under periodic loading, the area enclosed by the hysteresis loop corresponds to the energy dissipated by friction [4]. Various studies have used Jenkins elements to model bolted joints [6, 7]. Others have used it to model the nonlinear contact friction dampers commonly employed in bladed disk systems in turbomachinery [8], belt drives and power transmission systems [9, 10] or particular academic test structures of interest [11]. Pairs of decoupled Jenkins elements have also been used to analyse multidimensional contact interfaces [12, 13, 14]. However, a single Jenkins element on its own can only capture macro-slip and cannot be used to represent micro-slip which characterizes dry friction in reality [15]. This limitation can be overcome by using a set of Jenkins elements in parallel, sometimes referred to as a Masing Model or parallel-series Iwan Model [5, 16, 17]. This approach has been successfully used to reproduce the hysteresis loops of bolted joints under different types of dynamic loads obtained from experiments or detailed

*john.hickey@tcd.ie
†tb267@cam.ac.uk

finite element models in numerous works [18, 19, 20, 21, 22, 23]. While more sophisticated and physically realistic models can be found in literature (for example [24, 25, 26]), the Jenkins model and its derivatives are a versatile and relatively straightforward way to represent dry friction and are therefore widely used in engineering analysis. They are particularly useful for modelling contact interfaces in models with larger numbers of degrees of freedom [27], where more detailed modelling of the friction interface is impractical. In particular, they are often used in lumped parameter models employed in the initial design stage to provide fundamental understanding of system behaviour with relatively low computational costs compared to detailed finite element models [28].

Despite their conceptual simplicity, dynamic analysis of a Jenkins element or Iwan element is not straightforward to perform, due to their discontinuous and hysteretic behaviour. The presence of hysteresis means that some consideration must be given to past loading history in any analysis strategy, while models with discontinuities are difficult to simulate since it is necessary to find the instant where the discontinuities occur [6, 29]. Most analyses in literature employ approaches where the nonlinearity is studied in the time domain [3, 30], for example using direct time integration or an alternating frequency-time type approach (e.g. [8]). In terms of alternative, potentially more efficient, frequency domain approaches, Kashani [31] demonstrated how the Harmonic Balance Method (HBM) [32] and equivalent linearization [33, 34] could be used to analyse a Jenkins element subjected to harmonic and random excitation respectively.

This paper considers the more complex case where systems involving Jenkins and Iwan elements are subjected to combined deterministic harmonic and random excitation. While many engineering vibration problems are approximated as systems that are either harmonically or randomly excited, in reality many dynamic systems are subjected to a combination of harmonic excitation and broadband noise. Examples of such systems include floating crane systems [35], turbine blades under turbulent flows [36] or energy harvesting devices [37]. When this loading scenario is encountered, the conventional analysis approach at present is to adopt Monte-Carlo time-integration methods. However, this can become prohibitively computationally expensive, especially when multiple Monte Carlo realizations are required to account for the random component of the excitation.

A number of attempts have been made to develop computational techniques to analyse this combined loading scenario more efficiently. However, these are often specific to a particular nonlinearity. For example [38, 39, 40, 41, 42] presented methods specifically for the Duffing oscillator, while [43, 44] developed approaches particular to the van der Pol oscillator. As presented in these studies, these approaches are not useful for representing dry friction as they are limited to viscous damping and do not consider stick-slip behaviour. In recent years, Spanos and co-workers [45, 46] have proposed a more versatile approach, based on a combination of equivalent linearization and HBM. The method is based on separating the response into deterministic harmonic and random components. HBM is then used to derive a set of equations for the deterministic response component as functions of the random response statistical moments. Equivalent linearization, with the equivalent linear matrices averaged over a harmonic loading period, is then applied to the random response component, giving another set of equations involving the amplitudes of the harmonic response and the statistical moments of the random response. Combining these two sets of equations leads to a system of coupled nonlinear algebraic equations which can be solved for the two response components. A specific application of this method to hysteretic nonlinearity was performed for an SDOF system incorporating a Bouc Wen type nonlinearity [46]. However, the Bouc Wen model is not widely employed in the modelling of joints, as non-physical model parameters make model calibration difficult [5]. It is also prone to displacement drift and the so-called non-closure of minor loops, where the hysteretic behaviour from small reversals in the displacement within a larger loading cycle is not captured correctly [47]. Hickey et al. [48] proposed an alternative equivalent linearization approach, termed a Time and Ensemble Expectation Method (EL-TEE). Compared to the approach proposed by Spanos et al. [45], the linearization is performed before the response is separated into random and harmonic components. This means there is one fewer parameter per nonlinearity in the linearization, which theoretically reduces precision but has the advantage of returning meaningful linearization coefficients which can provide further insight into system behaviour.

This paper presents an extension of this approach to analyse systems with dry friction represented by Jenkins or parallel-series Iwan elements. This represents a flexible, computationally cheap, and interpretable method to analyse the response of friction nonlinearities. The paper begins by providing a brief overview of this analysis approach (Section 2). It then introduces the Jenkins and Iwan elements and details how the EL-TEE method is applied for these nonlinearities (Section 3 and 4). The key novelty is the use of a so-called auxiliary harmonic response to define the hysteresis loop and derive analytical solutions in the presence of a random excitation component. A number of example applications are shown, where it is demonstrated that the approach can approximate the key results of time integration at a much-reduced computational cost.

2 Time and Ensemble Expectation Approach

The equation of motion describing the response of a nonlinear system with a velocity and displacement dependent nonlinearity can be written as:

$$\mathbf{M}\ddot{\mathbf{v}} + \mathbf{C}\dot{\mathbf{v}} + \mathbf{K}\mathbf{v} + \mathbf{f_{nl}}(\mathbf{v}, \dot{\mathbf{v}}) = \mathbf{p} \tag{1}$$

where $\mathbf{M}$, $\mathbf{C}$ and $\mathbf{K}$ are the mass, damping and stiffness matrices respectively, $\mathbf{f_{nl}}(\mathbf{v}, \dot{\mathbf{v}})$ is the nonlinear restoring force, $\mathbf{p}$ is the excitation and $\mathbf{v}$ is the displacement.

Assuming a zero-mean load and response, Eq. (1) can be approximated using an equivalent linear system:

$$\mathbf{M}\ddot{\mathbf{v}} + \mathbf{C}\dot{\mathbf{v}} + \mathbf{K}\mathbf{v} + \mathbf{C^e}\dot{\mathbf{v}} + \mathbf{K^e}\mathbf{v} = \mathbf{p} \tag{2}$$

where $\mathbf{C^e}$ and $\mathbf{K^e}$ are equivalent linear damping and stiffness matrices respectively. The zero-mean assumption can be relaxed (see [48]) but is used here because it represents the majority of cases and simplifies the analysis. The error in the linearization, $\boldsymbol{\varepsilon}$, is defined as the difference between Eq. (1) and its linearized counterpart Eq. (2):

$$\boldsymbol{\varepsilon} \equiv \mathbf{f_{nl}}(\mathbf{v}, \dot{\mathbf{v}}) - \mathbf{C^e}\dot{\mathbf{v}} - \mathbf{K^e}\mathbf{v} \tag{3}$$

The system is assumed to be excited by a stationary random force plus a deterministic harmonic force of period T and frequency Ω. To minimize the error in the linearization, a cost function J is introduced. This cost function is defined as the expected value (i.e. the ensemble-expectation) of the sum of squares of the error averaged over one excitation period of the deterministic excitation component (i.e. the time-expectation):

$$min\left(J = \frac{1}{T}\int_0^T E[\boldsymbol{\varepsilon}^T\boldsymbol{\varepsilon}]\,dt\right) \tag{4}$$

which is equivalent to:

$$min\left(J = \frac{1}{T}\int_0^T E[\varepsilon_1^2 + \varepsilon_2^2 + \cdots + \varepsilon_n^2]\,dt\right) \tag{5}$$

where ε_n^2 is the n^th element in the vector $\boldsymbol{\varepsilon}$, defined by Eq. (3). As linearization is performed across the ensemble and over time, the proposed approach is described as a Time and Ensemble Expectation (EL-TEE) method. The minimization is performed with respect to each element of the equivalent stiffness matrix and equivalent damping matrix:

$$\int_0^T \frac{\partial}{\partial K^e_{i,j}} E[\boldsymbol{\varepsilon}^T\boldsymbol{\varepsilon}]\,dt = 0 \tag{6}$$

$$\int_0^T \frac{\partial}{\partial C^e_{i,j}} E[\boldsymbol{\varepsilon}^T\boldsymbol{\varepsilon}]\,dt = 0 \tag{7}$$

where $K^e_{i,j}$ and $C^e_{i,j}$ are the (i, j) elements of the matrices $\mathbf{K^e}$ and $\mathbf{C^e}$ respectively. This gives the following linearization equations:

$$\int_0^T E[\mathbf{f_{nl}}\mathbf{v^T}]\,dt = \mathbf{K^e}\int_0^T E[\mathbf{v}\mathbf{v^T}]\,dt + \mathbf{C^e}\int_0^T E[\dot{\mathbf{v}}\mathbf{v}^T]\,dt \tag{8}$$

$$\int_0^T E[\mathbf{f_{nl}}\dot{\mathbf{v}}^\mathbf{T}]\,dt = \mathbf{K^e}\int_0^T E[\mathbf{v}\dot{\mathbf{v}}^\mathbf{T}]\,dt + \mathbf{C^e}\int_0^T E[\dot{\mathbf{v}}\dot{\mathbf{v}}^T]\,dt \tag{9}$$

These linearization expressions can be expressed as a single system of equations:

$$\int_0^T E\left[\begin{Bmatrix}\mathbf{v}\\ \dot{\mathbf{v}}\end{Bmatrix}\mathbf{f_{nl}}^T\right]dt = \left[\int_0^T E\begin{bmatrix}\mathbf{v}\mathbf{v^T} & \dot{\mathbf{v}}\mathbf{v}^T\\ \mathbf{v}\dot{\mathbf{v}}^T & \dot{\mathbf{v}}\dot{\mathbf{v}}^T\end{bmatrix}dt\right]\begin{Bmatrix}\mathbf{K^e}^T\\ \mathbf{C^e}^T\end{Bmatrix} \tag{10}$$

The linearization matrices obtained by solving Eq. (10) can then be applied in Eq. (2) to calculate the response of the equivalent linear system. This is done by assuming that the response is stable such that both the response and excitation can be separated into harmonic and zero-mean random components, termed $\mathbf{v_h}$ and $\mathbf{v_r}$ and $\mathbf{p_h}$ and $\mathbf{p_r}$. This allows Eq. (2) to be re-written as:

$$\mathbf{M}(\ddot{\mathbf{v}}_\mathbf{h} + \ddot{\mathbf{v}}_\mathbf{r}) + (\mathbf{C} + \mathbf{C^e})(\dot{\mathbf{v}}_\mathbf{h} + \dot{\mathbf{v}}_\mathbf{r}) + (\mathbf{K} + \mathbf{K^e})(\mathbf{v_h} + \mathbf{v_r}) = \mathbf{p_h} + \mathbf{p_r} \tag{11}$$

Taking expectations across the ensemble gives the following expression describing the harmonic response:

$$\mathbf{M}\ddot{\mathbf{v}}_\mathbf{h} + (\mathbf{C} + \mathbf{C^e})\dot{\mathbf{v}}_\mathbf{h} + (\mathbf{K} + \mathbf{K^e})\mathbf{v_h} = \mathbf{p_h} \tag{12}$$

Eq. (12) can be solved using the standard steady-state solution for a harmonically driven oscillator with $\mathbf{p_h} = \mathbf{P_h}e^{i\Omega t}$ and $\mathbf{v_h} = \mathbf{V_h}e^{i\Omega t}$ (implicitly taking the real part):

$$\mathbf{V_h(i\Omega)} = \left[-\Omega^2\mathbf{M} + i\Omega(\mathbf{C} + \mathbf{C^e}) + (\mathbf{K} + \mathbf{K^e})\right]^{-1}\mathbf{P_h} \tag{13}$$

where $\mathbf{P_h}$ and $\mathbf{V_h}$ are the complex amplitudes of the harmonic excitation and response respectively. Subtracting Eq. (12) from Eq. (11) leaves the equation governing the random response component:

$$\mathbf{M}\ddot{\mathbf{v}}_\mathbf{r} + (\mathbf{C} + \mathbf{C^e})\dot{\mathbf{v}}_\mathbf{r} + (\mathbf{K} + \mathbf{K^e})\mathbf{v_r} = \mathbf{p_r} \tag{14}$$

Standard frequency-domain linear random vibration theory can be used to solve Eq. (14) and obtain the cross-spectral density matrix of the random response component. The covariance matrix of the response can then be obtained by integrating each element of this matrix across all frequencies. Alternatively, if it is assumed that the random excitation is Gaussian white noise with a spectral density matrix $mathbfS_0$, the covariance matrix of the random response component can be obtained directly by solving the Lyapunov Equation describing the response of a randomly loaded oscillator [33]:

$$\mathbf{AV^T} + \mathbf{VA^T} = -\mathbf{G} \tag{15}$$

where:

$$\mathbf{A} = \begin{bmatrix} \mathbf{0} & \mathbf{I} \\ -(\mathbf{K} + \mathbf{K^e}) & -(\mathbf{C} + \mathbf{C^e}) \end{bmatrix} \tag{16}$$

where $\mathbf{I}$ is the identity matrix. $\mathbf{V}$ is the covariance matrix of the random response component:

$$\mathbf{V} = \begin{bmatrix} E[\mathbf{v_r}\mathbf{v_r^T}] & E[\mathbf{v}_r\dot{\mathbf{v}}_\mathbf{r}^T] \\ E[\dot{\mathbf{v}}_\mathbf{r}\mathbf{v_r}^T] & E[\dot{\mathbf{v}}_\mathbf{r}\dot{\mathbf{v}}_\mathbf{r}^T] \end{bmatrix} \tag{17}$$

and $\mathbf{G}$ is given by:

$$\mathbf{G} = \begin{bmatrix} \mathbf{0} & \mathbf{0} \\ \mathbf{0} & 2\pi\mathbf{S_0} \end{bmatrix} \tag{18}$$

This Lyapunov Equation approach avoids the need for integration over frequency, thus improving computational efficiency compared to the more generally applicable spectral approach. Combining Eq. (10), Eq. (13) and Eq. (15) allows the response of the system to be calculated by solving the nonlinear simultaneous equations:

$$\begin{bmatrix} E[\mathbf{v_r}\mathbf{v_r^T}] & E[\mathbf{v}_r\dot{\mathbf{v}}_\mathbf{r}^T] \\ E[\dot{\mathbf{v}}_\mathbf{r}\mathbf{v_r}^T] & E[\dot{\mathbf{v}}_\mathbf{r}\dot{\mathbf{v}}_\mathbf{r}^T] \end{bmatrix} = Lyapunov(\mathbf{A}, \mathbf{G}) \tag{19a}$$

$$\mathbf{v_h(i\Omega)} = \left[-\Omega^2\mathbf{M} + i\Omega(\mathbf{C} + \mathbf{C^e}) + (\mathbf{K} + \mathbf{K^e})\right]^{-1}\mathbf{P_h} \tag{19b}$$

$$\int_0^T E\left[\begin{Bmatrix}\mathbf{v} \\ \dot{\mathbf{v}}\end{Bmatrix}\mathbf{f_{nl}}^T\right]dt = \left[\int_0^T E\begin{bmatrix}\mathbf{v}\mathbf{v^T} & \dot{\mathbf{v}}\mathbf{v}^T \\ \mathbf{v}\dot{\mathbf{v}}^T & \dot{\mathbf{v}}\dot{\mathbf{v}}^T\end{bmatrix}dt\right]\begin{Bmatrix}\mathbf{K^e}^T \\ \mathbf{C^e}^T\end{Bmatrix} \tag{19c}$$

The Lyapunov Equation can be solved easily using standard solvers, for example the inbuilt `Lyap` function in `Matlab`. The system of equations in Eq. (19) can be solved using nonlinear solvers, such as the `fsolve` function in `Matlab`. Furthermore, when evaluating the expectations in Eq. (19.c), it can be assumed that the random response component $\mathbf{v_r}$ follows a Gaussian distribution. Finally, the root mean square value of the combined dynamic displacement (once the deterministic component of the starting transient has decayed) for degree of freedom p can be shown to be:

$$v_{rms,p} = \sqrt{\frac{V_{h,p}^2}{2} + E[v_{r,p}v_{r,p}]} \tag{20}$$

3 Description of the Nonlinearity

The general method presented in Section 2 is now applied to the case where the nonlinearity includes friction. The Jenkins element model involves sticking and slipping states, as shown in Figure 1(a). During sticking the contact is purely elastic, while in sliding the contact point starts to slide and the nonlinear force is equal to a constant limiting friction force that opposes the direction of sliding. This behaviour can be represented by the set of Equations in Eq. (21).

$$f(v,\dot{v}) = k_s\Big(v + (V_y - V_{max})\Big); \qquad if \quad \dot{v} > 0, v < 2V_y + V_{max} \tag{21.a}$$

$$f(v,\dot{v}) = k_s V_y; \qquad if \quad \dot{v} > 0, v > 2V_y + V_{max} \tag{21.b}$$

$$f(v,\dot{v}) = k_s\Big(v - (V_y - V_{max})\Big) \qquad if \quad \dot{v} < 0, v > -2V_y + V_{max} \tag{21.c}$$

$$f(v,\dot{v}) = -k_s V_y \qquad if \quad \dot{v} < 0, v < -2V_y + V_{max} \tag{21.d}$$

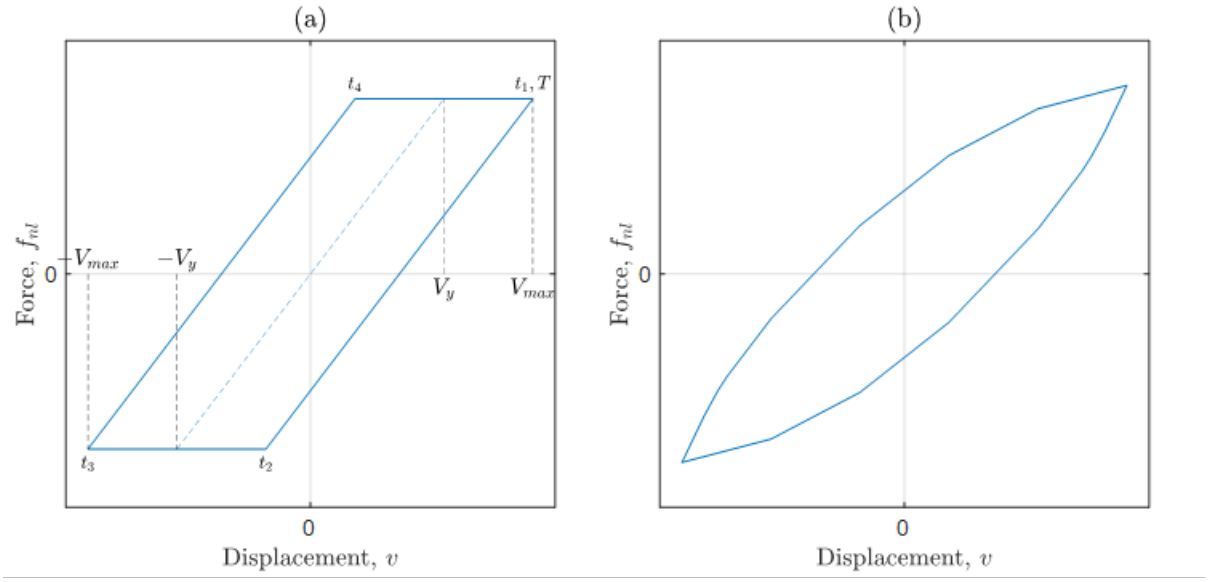

Fig. 1: (a) Hysteresis loop for a Jenkins element, showing notation employed in the study. t_x represents the time at which the change between branches occurs and T is the time required for one full cycle. (b) Example hysteresis loop for a parallel-series Iwan element formed form a combination of 8 Jenkins elements in parallel.

The parallel-series Iwan model, as discussed, employs a series of Jenkins elements in parallel, which allows a more realistic representation of the dry friction to be created. Figure 1(b), shows an example of the type hysteresis loop that can be obtained with increasing numbers of elements.

In order to apply the linearization approach proposed it is necessary to evaluate the integrals in Eq. (19.c). As shown in Appendix A, the integrals on the right-hand side can be shown to be:

$$\int_0^T E[v_i v_j]\,dt = E[v_{r,i}v_{r,j}] + V_{h,i}V_{h,j}\frac{1}{2}\cos(\phi_i - \phi_j) \tag{22.a}$$

$$\int_0^T E[v_i \dot{v}_j]\,dt = E[v_{r,i}\dot{v}_{r,j}] + V_{h,i}V_{h,j}\Omega\frac{1}{2}\sin(\phi_i - \phi_j) \tag{22.b}$$

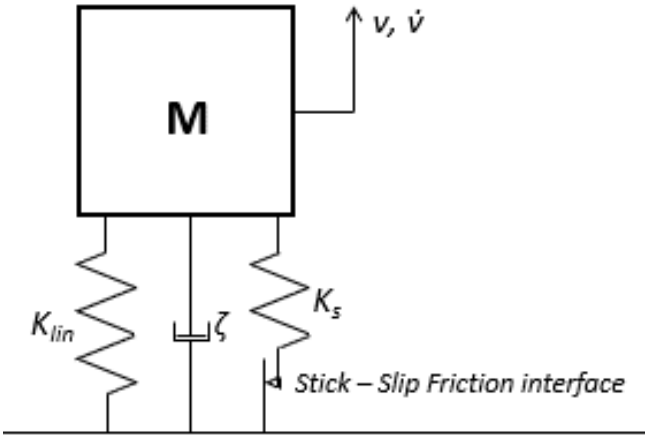

Fig. 2: Illustration of an SDOF oscillator connected to a Jenkins element.

$$\int_0^T E[\dot{v}_i v_j]\,dt = E[\dot{v}_{r,i} v_{r,j}] + V_{h,i} V_{h,j} \Omega \frac{1}{2} \sin(\phi_i - \phi_j) \tag{22.c}$$

$$\int_0^T E[\dot{v}_i \dot{v}_j]\,dt = E[\dot{v}_{r,i} \dot{v}_{r,j}] + V_{h,i} V_{h,j} \Omega^2 \frac{1}{2} \cos(\phi_i - \phi_j) \tag{22.d}$$

where the subscripts i and j refer to degrees of freedom. The integrals on the left-hand side are non-trivial to compute for the friction nonlinearity described by Eq. (21), due to the presence of a random response component. However, if the response is assumed to be periodic, then these terms can be shown to be:

$$\begin{aligned}\int_0^T E[v_i f_{nl,j}]\,dt = &\sum_k 2\Big(k_s V_y \frac{V_{h,i}}{\Omega}\big(\cos(\Omega t_3 + \phi_i) - \cos(\Omega t_2 + \phi_i)\big)\Big) \\ &+2\Big(k_s\big(E[v_{r,i} v_{r,j}] - E[v_{r,i} v_{r,k}]\big)\big(t_2 - t_1\big) + k_s\big(a_{i,j}(t_2, t_1) - a_{i,k}(t_2, t_1)\big) \\ &+k_s \frac{(V_y - V_{max}) V_{h,i}}{\Omega}\big(\cos(\Omega t_2 + \phi_i) - \cos(\Omega t_1 + \phi_i)\big)\Big)\end{aligned} \tag{23}$$

$$\begin{aligned}\int_0^T E[\dot{v}_i f_{nl,j}]\,dt = &\sum_k 2\Big(k_s V_y V_{h,i}\big(\sin(\Omega t_3 + \phi_i) - \sin(\Omega t_2 + \phi_i)\big)\Big) \\ &+2\Big(k_s\big(E[\dot{v}_{r,i} v_{r,j}] - E[\dot{v}_{r,i} v_{r,k}]\big)\big(t_2 - t_1\big) + k_s\big(b_{i,j}(t_2, t_1) - b_{i,k}(t_2, t_1)\big) \\ &+k_s (V_y - V_{max}) V_{h,i}\big(\sin(\Omega t_2 + \phi_i) - \sin(\Omega t_1 + \phi_i)\big)\Big)\end{aligned} \tag{24}$$

where the subscript k refers to any degree of freedom connected via a Jenkins element to degree of freedom j (see illustration in Figure 10). For a single degree of freedom (SDOF) oscillator, such as the system illustrated in Figure 2, $v_k = 0$. In Eq. (23) and (24) the functions a_{ij} and b_{ij} represent the integral of the product of two cosines and two sines respectively, such that:

$$a_{i,j}(t_1, t_2) = \int_{t_1}^{t_2} v_{hi} v_{h,j}\,dt = \int_{t_1}^{t_2} V_{hi} \cos(\Omega t + \phi_i) V_{h,j} \cos(\Omega t + \phi_j)\,dt \tag{25}$$

$$b_{i,j}(t_1, t_2) = \int_{t_1}^{t_2} \dot{v}_{hi} \dot{v}_{h,j}\,dt = \Omega^2 \int_{t_1}^{t_2} V_{hi} \sin(\Omega t + \phi_i) V_{h,j} \sin(\Omega t + \phi_j)\,dt \tag{26}$$

Eq. (23) and (24) provide analytical expressions to evaluate the integrals in Eq. (19) for the Jenkins element. This is preferable to a numerical approach, both as it saves computational time, and avoids the need to synthesize a random load or response as part of the solution algorithm. The t_1 to t_3 terms in Eq. (23) and (24) describe the times corresponding to the transitions between the different branches of the nonlinearity, as illustrated in Figure 1(a). The symmetry of the hysteresis loop for harmonic displacement means that the integrals from t_3 to T are the same as from t_1 to t_3, which explains the absence of t_4 and T terms from Eq. (23) and Eq. (24). The process of evaluating the required transition times in the presence of both random and harmonic response components is discussed in the following section.

4 Application to Friction Nonlinearity

4.1 SDOF System with Jenkins Element

The method is first applied to the single degree of freedom oscillator with a Jenkins element that was illustrated in Figure 1. The system is assigned unit mass and linear stiffness with 5% damping, i.e. $M = 1kg$, $K = 1N/m$ and $C = 0.1Ns/m$ (giving $\zeta = 0.05$). The Jenkins element is assigned a spring stiffness, $k_s = 0.3N/m$. The analysis is first performed for the case of purely harmonic excitation (i.e. with no random excitation) with unit amplitude. In this case the maximum displacement defining the hysteresis loop, V_{max} (see Figure 1(a)), is equal to the amplitude of the steady state harmonic response, V_h. This allows the times of transition between the various branches of the hysteresis loop, as illustrated in Figure 1(a), to be evaluated as:

$$t_1 = 0 \tag{27.a}$$

$$t_2 = \frac{1}{\Omega}\left(\cos^{-1}\left(\frac{2V_y - V_h}{V_h}\right)\right) \tag{27.b}$$

$$t_3 = \frac{T}{2} \tag{27.c}$$

$$t_4 = t_1 + \frac{T}{2} \tag{27.d}$$

Assuming that the hysteresis loop is harmonic with the transition times as per Eq. (27) allows the expressions in Eq. (23) and (24) to be evaluated. In turn, the coupled nonlinear equations in Eq. (19) can be solved, in this case using a Newton-Raphson scheme implemented in fsolve in Matlab.

The results of this process for the sample system considered are presented in Figure 3, which shows the variation in RMS displacement with harmonic excitation frequency obtained from this process for three Jenkins elements with different slip conditions. The Jenkins elements are characterized by the ratio of the contact forces at the point of slip, μ_N, to the amplitude of the harmonic excitation force, P_h. Benchmark results obtained from a Newmark-Beta time integration scheme are also presented for comparison.

Newmark-Beta is a numerical solution scheme for second order differential equations, that is widely employed in structural dynamics problems [49]. In this study the well-known linear acceleration version of the scheme ($\gamma = 1/2$, $\beta = 1/6$ using conventional notation), with a sufficiently small timestep to ensure numerical stability, is adopted. For application to a nonlinear Jenkins element, an iterative Newton Raphson solution procedure is employed. Each iteration involves evaluating the tangent stiffness matrix, calculating the increment in displacement and force in the Jenkins element, assessing whether the Jenkins element is in the stick or slip condition and calculating the residual force before advancing to the next timestep if the difference between internal and applied force is less than an acceptable tolerance.

Additionally, Figure 3 also shows the response in two limiting cases: the ‘full stick’ case where the damper does not slip at all and behaves like an additional spring element; and the ‘full slip’ case when the damper always slips and offers no additional force. It can be seen that the results obtained from the proposed EL-TEE approach are essentially indistinguishable from those obtained from time integration. This demonstrates that the approach works as expected

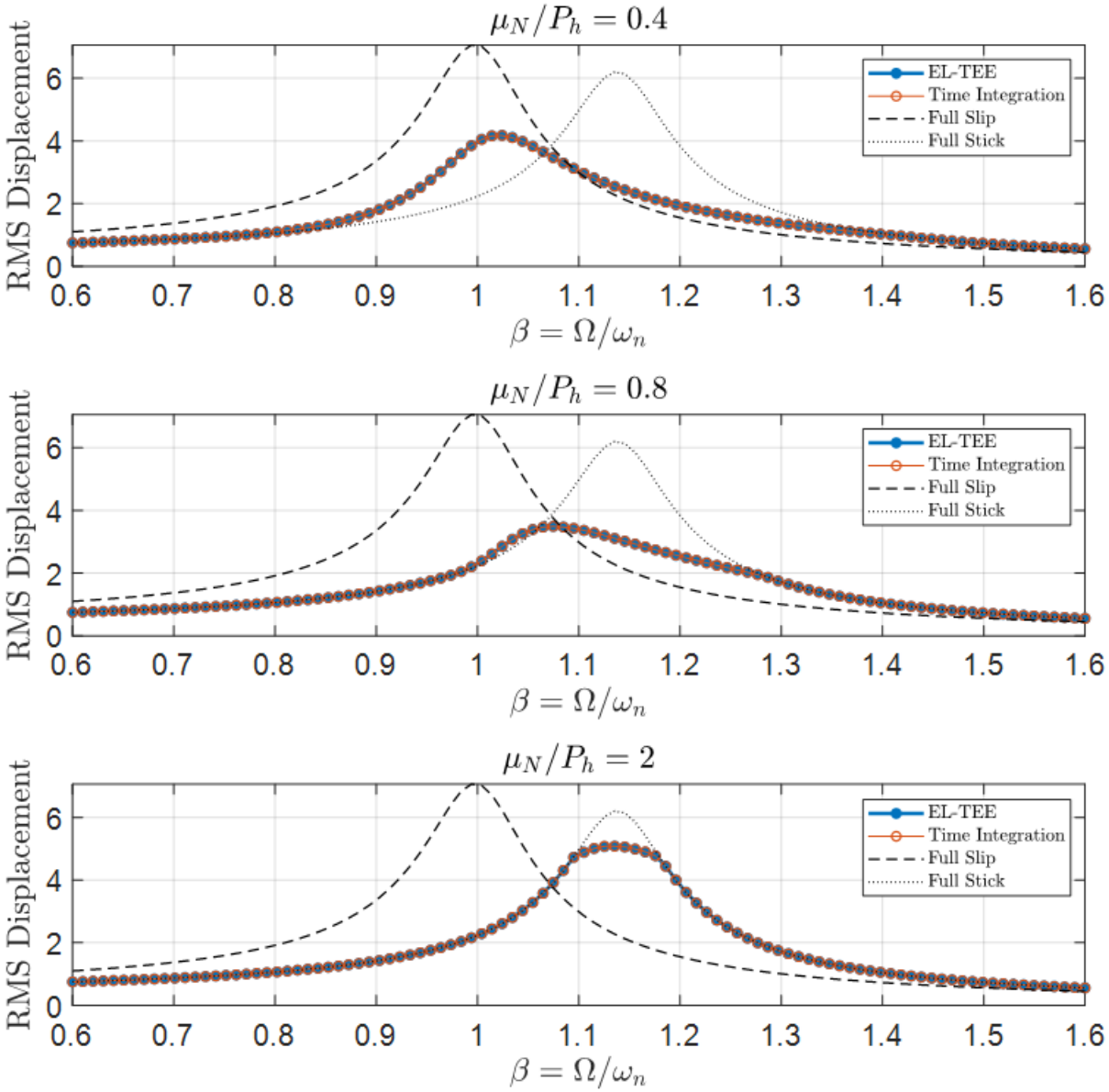

Fig. 3: Comparison between RMS displacement response calculated using the proposed EL-TEE approach and time integration for a SDOF system connected to a Jenkins element subjected to harmonic excitation across a range of excitation frequencies.

in the base-case scenario without random excitation. Note that for purely harmonic excitation the method is equivalent to HBM with a single term [31].

Figure 4 presents results for combined harmonic and random excitation. Here, the random excitation component is white noise with a spectral density of $S_0 = 0.32N^2s$. From Figure 4, it can be seen that while the EL-TEE method appears to capture the general trends seen in time integration, there is some discrepancy between the results obtained from the two approaches.

This discrepancy can be attributed to the assumption that that the transition times in Eq. (23) and (24) are approximated based solely on the harmonic response component, as per Eq. (27). This assumption introduces error in the presence of random excitation, which grows as the strength of the random excitation component is increased. The reason for this discrepancy is illustrated in Figure 5, which shows the response of an example SDOF system including a Jenkins element with $\mu_N/P_h = 0.4$ (i.e. the system shown in the first subplot of Figure 4) to combined excitation with harmonic force of unit amplitude and frequency $\Omega = 1.5s^{-1}$ and gaussian white noise of spectral density $S_0 = 0.32N^2s$. The response for a single Monte Carlo realization calculated using the Newmark Beta algorithm is shown in blue. It can be observed here that slip and energy dissipation occurs in this case. However, the amplitude

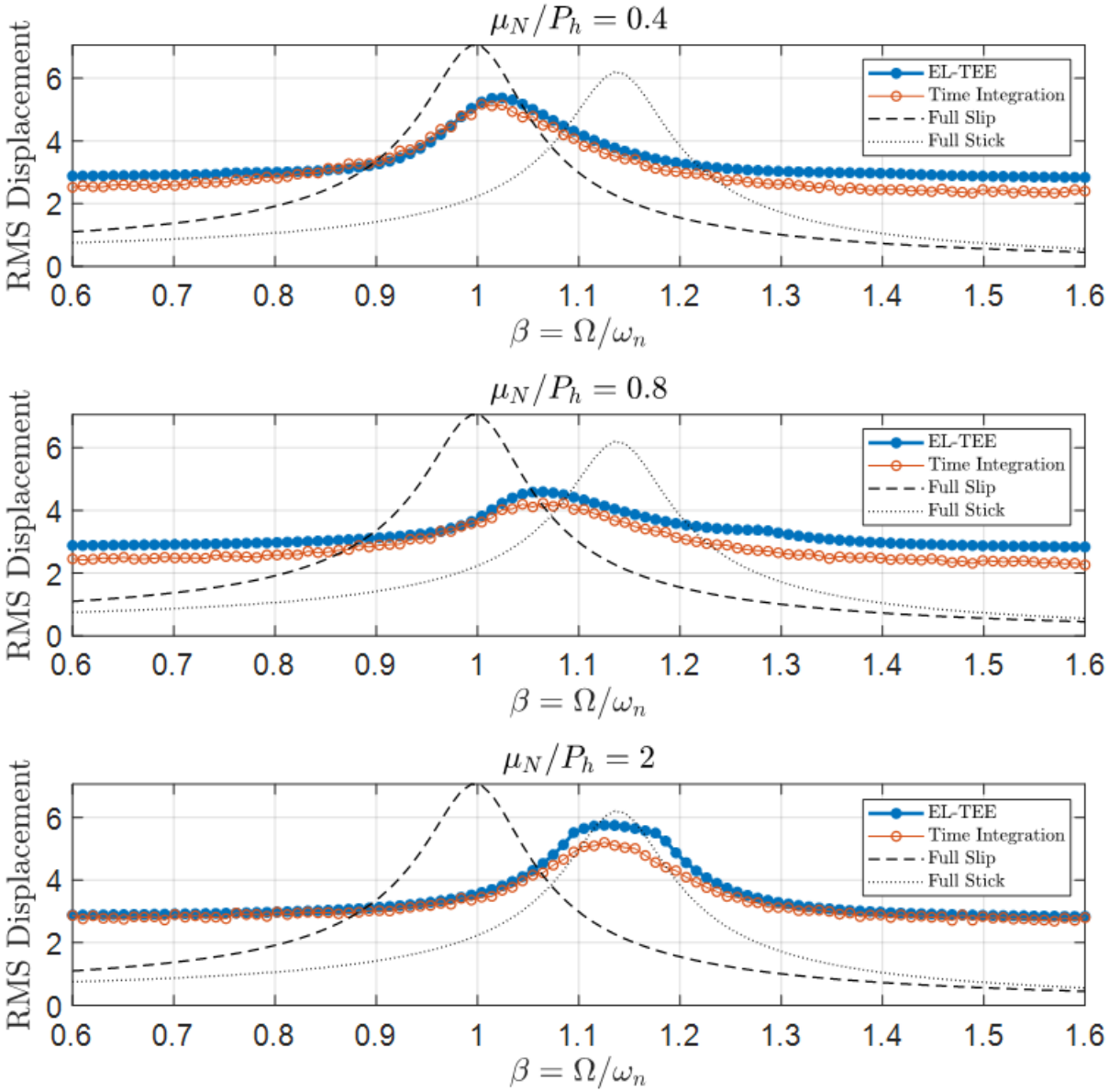

Fig. 4: Comparison between RMS displacement response calculated using the proposed EL-TEE approach and time integration for a SDOF system connected to a Jenkins element subjected to combined random and harmonic excitation across a range of harmonic excitation frequencies. The integrals in the EL-TEE approach are calculated assuming the nonlinear force is defined by the amplitude of the harmonic excitation component only.

of the harmonic response component obtained from EL-TEE is less than the displacement corresponding to slip. If this harmonic response is assumed to be the maximum response in the definition of the hysteresis loop, the system is analysed as if it remains in the 'stick' state. This can be seen in the upper two subfigures in Figure 5, where the force displacement curve remains linear. Therefore, if the representation of the nonlinear force in the EL-TEE method is based on just the harmonic response, and the harmonic amplitude is not large enough to cause slip, this energy dissipation is not captured.

In order to overcome this issue, an approximation is made that still allows the integrals within Eq. (23) and (24) to be obtained analytically. It is assumed that the hysteresis loop is defined by an auxiliary harmonic displacement, denoted $v_{aux} = v_{aux}\sin(\Omega t + \theta)$, with an RMS value equal to the RMS of the combined harmonic and random response such that:

$$V_{aux} = \sqrt{V_h^2 + 2E[v_r^2]} \tag{28}$$

The use of an auxiliary harmonic displacement with this RMS value is justified on the basis that the expected energy dissipation is equal to that of the true combined displacement. In turn, this auxiliary harmonic displacement can be used to evaluate the transition times in Eq. (23) and (24).

$$t_1 = 0 \tag{29.a}$$
$$t_2 = \frac{1}{\Omega}\left(\cos^{-1}\left(\frac{2V_y - V_{aux}}{V_{aux}}\right)\right) \tag{29.b}$$

Graphically, this idea is illustrated in Figure 5. When the auxiliary harmonic approach is adopted, the occurrence of slip and energy dissipation is captured, as shown in the lower subfigures. This approach allows the integrals to be evaluated analytically whilst maintaining the ability to capture energy dissipation due to slipping arising from the random response component.

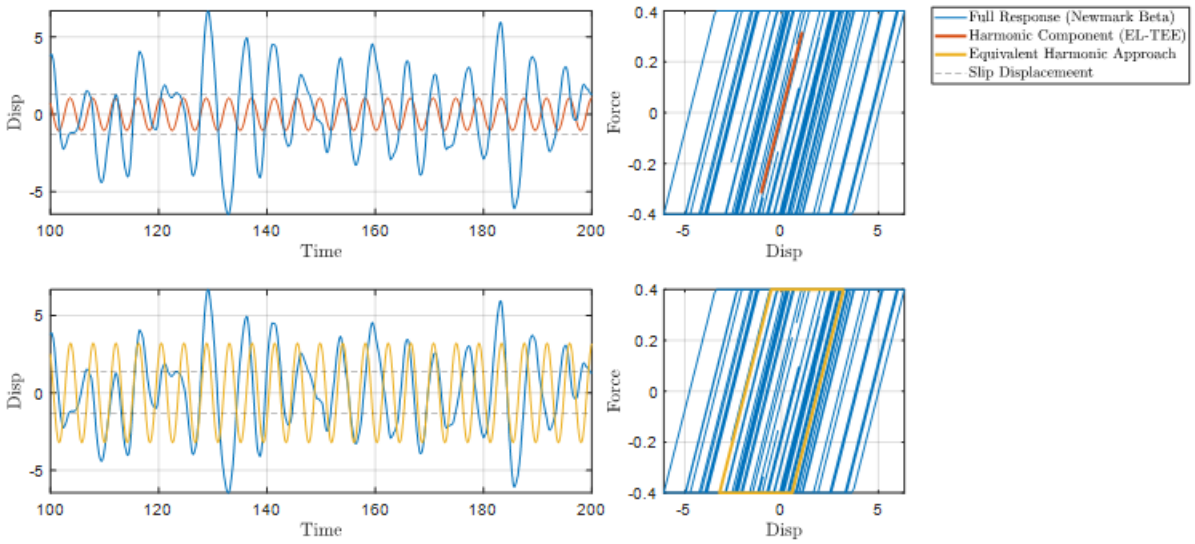

Fig. 5: Demonstration of the difference between the hysteresis loop calculated using the harmonic response and the auxiliary harmonic approach.

Considering the same system analysed in Figure 5, Figure 6(a) compares the cumulative energy dissipated where response is calculated using time integration and the simplified auxiliary harmonic hysteresis loop over 500 harmonic excitation periods. Over this time, it is apparent that the cumulative energy dissipation observed from the two approaches is quite similar. For the particular example case shown, the average energy dissipated over one harmonic loading cycle calculated from time integration is equal to 3.00 Nm per cycle, while the equivalent value from the auxiliary harmonic approach is 2.99 Nm per cycle. The similarity of these numbers demonstrates that the auxiliary harmonic approximation is an effective way to represent the average dissipative behaviour of the Jenkins element reasonably well, whilst maintaining the ability to analyse the nonlinearity analytically. Figure 6(b) shows how the values of energy dissipated per cycle change as the spectral density of the random loading component is increased. For this example system, it can be seen that at lower spectral densities the dissipated energies estimated using the auxiliary harmonic are quite close to those from time integration, with the values overestimated by roughly 10% by the auxiliary harmonic approach at higher spectral densities. Figure 6(c) shows the percentage error in the estimation of the RMS displacement calculated using the proposed auxiliary harmonic approach across this range of excitation amplitudes. It is observed that RMS displacement is underestimated compared to time integration, which is a consequence of the overestimation of the energy dissipation. However, the magnitude of this error is in the order of 5% or less, demonstrating the effectiveness of the proposed linearization.

Figure 7 demonstrates the performance of the approach across a range of harmonic excitation frequencies. The results of the same analyses as Figure 4 are presented, but this time with the hysteresis loop in the Equivalent Linearization approximated using the auxiliary harmonic response. This means that the approach is able to capture the cases where the random response component causes slip and energy dissipation, which allows a closer match with the results of time integration to be obtained.

Figure 7 also presents the time required to complete the analysis at all harmonic excitation frequencies considered via the EL-TEE and the Newmark approach. It can be seen that the EL-TEE approach takes approximately half a

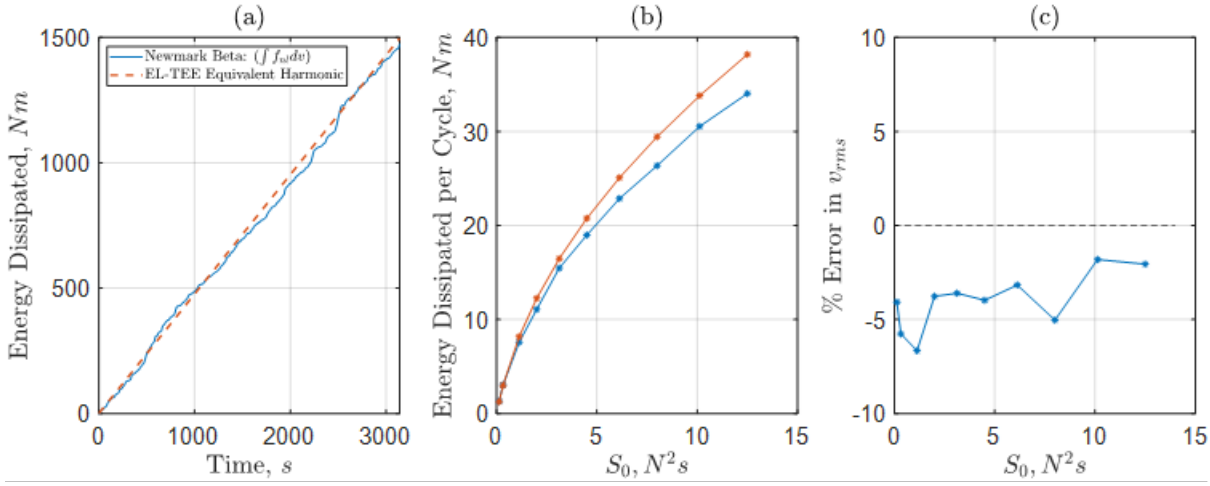

Fig. 6: (a)Comparison between the cumulative energy dissipation for the example case presented in Figure 5, calculated using results from time integration and from EL-TEE using the auxiliary harmonic approach; (b) Comparison of energy dissipated per cycle for the same example system for random loading components of increasing spectral density; (c) percentage error in the RMS displacement for different random loading components.

second to generate the results presented, whereas over 200s are required to complete the Monte Carlo realizations. This demonstrates the computational efficiency of the proposed calculation approach.

The approach also returns equivalent stiffness and damping terms, as presented in Figure 8. These terms come directly from the solution to Eq. (19.c). and can be used to assess the impact of the Jenkins element on the oscillator. For example, it can be seen that at harmonic excitation of $\beta = 0.6$ for the μ_N/P_h of 0.8, the system behaves like a linear system with frequency $\omega_n = 1.11 rad/s$ and viscous damping of 8%.

The effectiveness of the linearization for a wide range of systems and loading scenarios is examined in Figure 9, which shows the absolute value of percentage difference in RMS response between results from the proposed approach and time integration realizations. As before, the system considered is assigned unit mass and linear stiffness and 5% damping, with results for a large number of different random excitations and contact forces at slip shown. It can be seen that the error is less than 10% for the vast majority of analyses performed, with values closer to 20% observed in a small number of cases. Considering the variation in error with the strength of the random excitation component, the proposed method is seen to perform best at the extremes when the response is dominated by either harmonic (for example in the $S_0 = 0.04 Ns^2$ case) or random components (for example in the $S_0 = 9.56 Ns^2$ case). Errors are greater when both response components are prevalent, for example in the $S_0 = 0.93 Ns^2$ case presented. Similarly, in terms of contact force at the point of slip, μ_N/P_h, errors tend to be more pronounced for intermediate values (e.g. $\mu_N/P_h = 4$), where the determination of whether slip occurs is challenging, rather than extreme values ($\mu_N/P_h = 0.25$ or $mu_N/P_h = 10$), where slip is either very likely or very unlikely to occur. However, overall, the level of error observed is relatively low, and the proposed linearization appears robust for higher random loading components.

While the results presented in Figure 6 and Figure 9 show that the proposed method performs well for quite a wide variety of scenarios, it should be borne in mind that, as presented here, the approach is limited to the Jenkins nonlinearity and to a single harmonic excitation with broadband white noise. For alternative nonlinearities or loading scenarios, like multi-harmonic excitation or band-limited noise, it is possible to envisage ways to adapt the approach, but this is beyond the scope of the present study.

4.2 4.2 MDOF system with Parallel-Series Iwan Element

Having demonstrated the application of the EL-TEE approach for a single Jenkins element, the approach can now be expanded to a parallel-series Iwan element. In this case the integrals described by Eq. (23) and Eq. (24) need to be summed over each individual Jenkins element, q, connecting degree of freedom j to degree of freedom k:

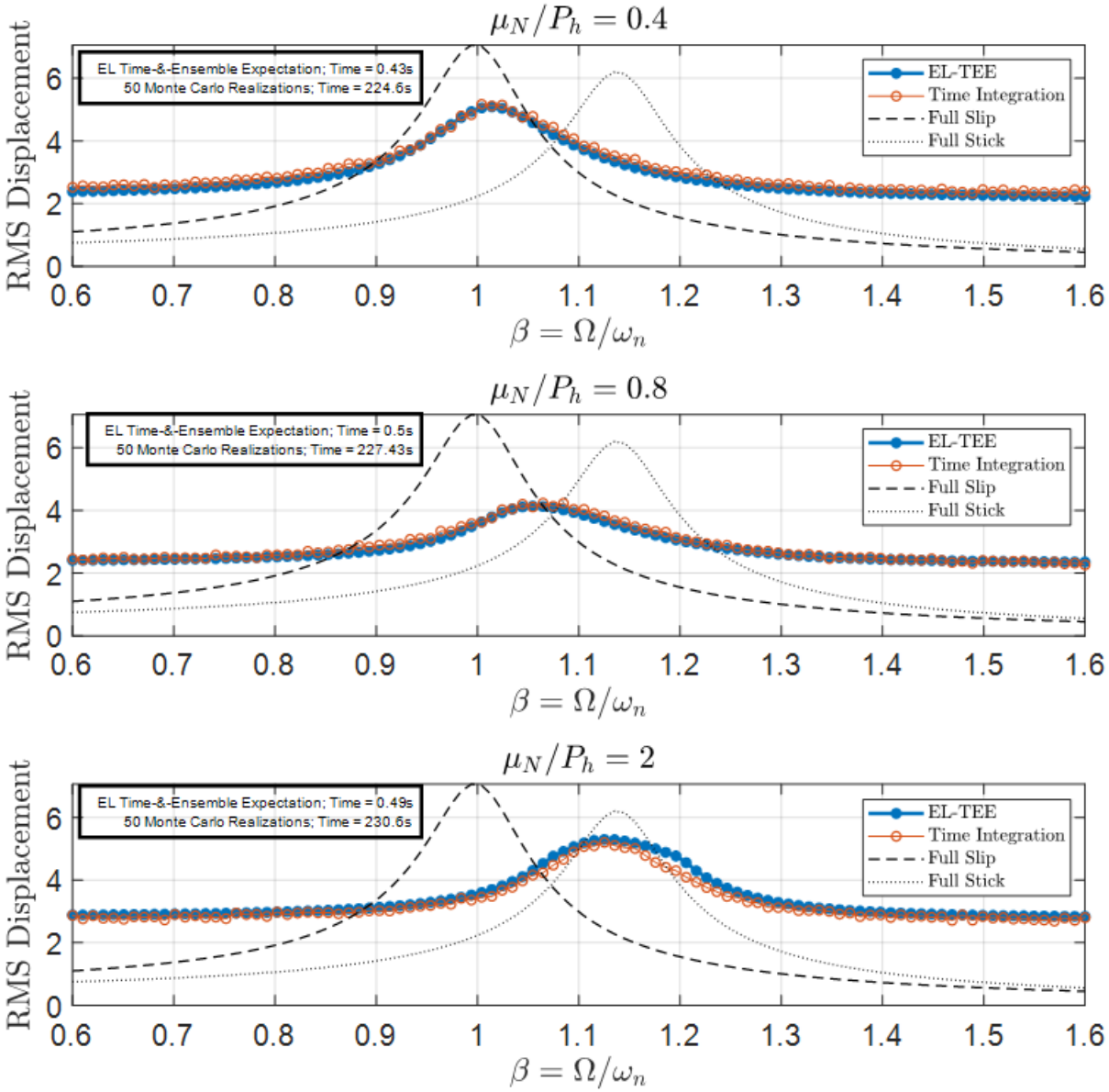

Fig. 7: Comparison of RMS displacement response calculated using the proposed EL-TEE approach and time integration for a SDOF system connected to a Jenkins element subjected to combined random and harmonic excitation across a range of harmonic excitation frequencies. The integrals in the EL-TEE approach are calculated assuming the nonlinear force is defined by an auxiliary harmonic displacement accounting for both random and harmonic loading components.

$$\int_0^T E[v_i f_{nl,j}]\,dt = \sum_k \sum_q 2\Big(k_{s,q} V_{y,q} \frac{V_{h,i}}{\Omega}\Big(\cos(\Omega t_{3,q} + \phi_i) - \cos(\Omega t_{2,q} + \phi_i)\Big)\Big)$$
$$+2\Big(k_{s,q}\Big(E[v_{r,i}v_{r,j}] - E[v_{r,i}v_{r,k}]\Big)\Big(t_{2,q} - t_{1,q}\Big) + k_{s,q}\Big(a_{i,j}(t_{1,q}, t_{2,q}) - a_{i,k}(t_{2,q}, t_{1,q})\Big) \tag{30}$$
$$+k_{s,q}\frac{(V_{y,q} - V_{max})V_{h,i}}{\Omega}\Big(\cos(\Omega t_{2,q} + \phi_i) - \cos(\Omega t_{1,q} + \phi_i)\Big)\Big)$$

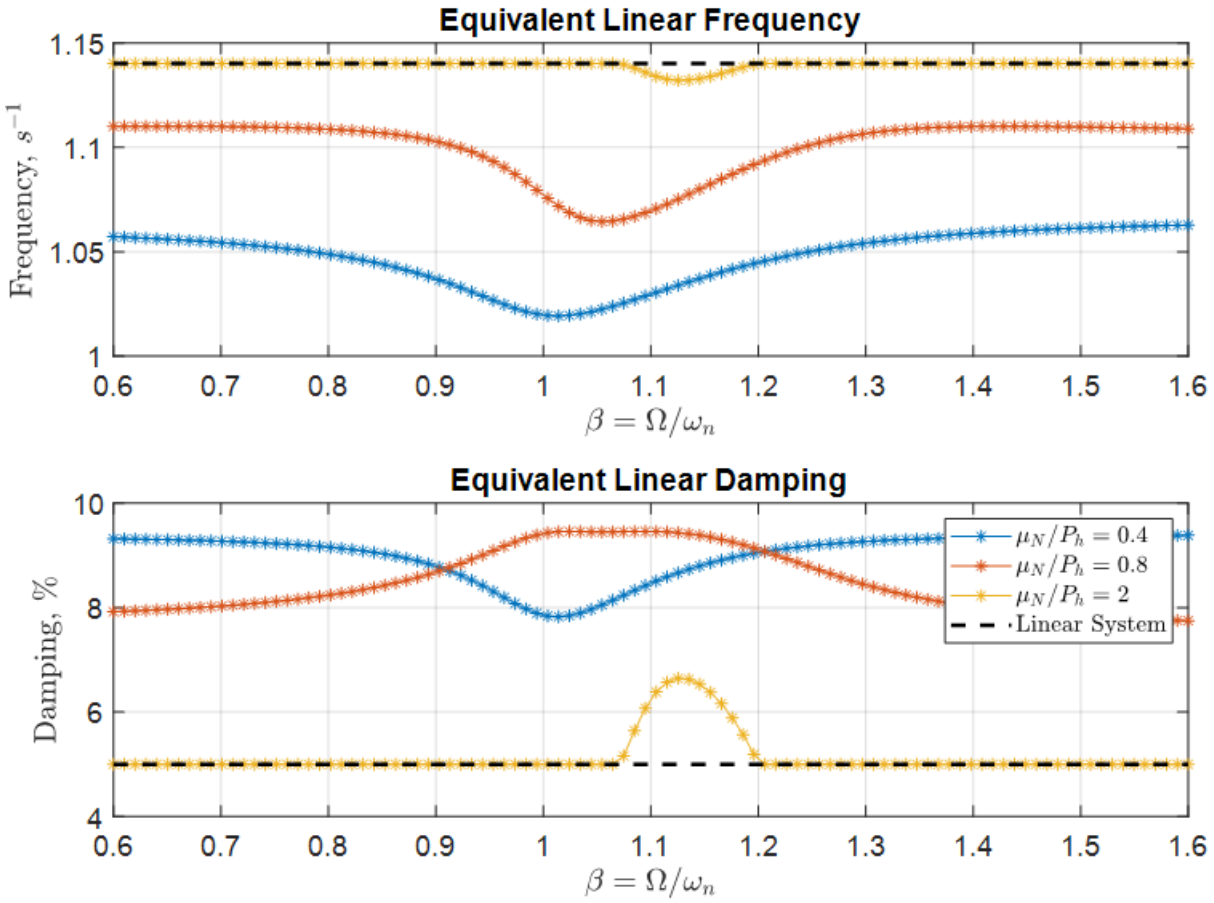

Fig. 8: Equivalent Linear Properties for systems analysed in Figure 7.

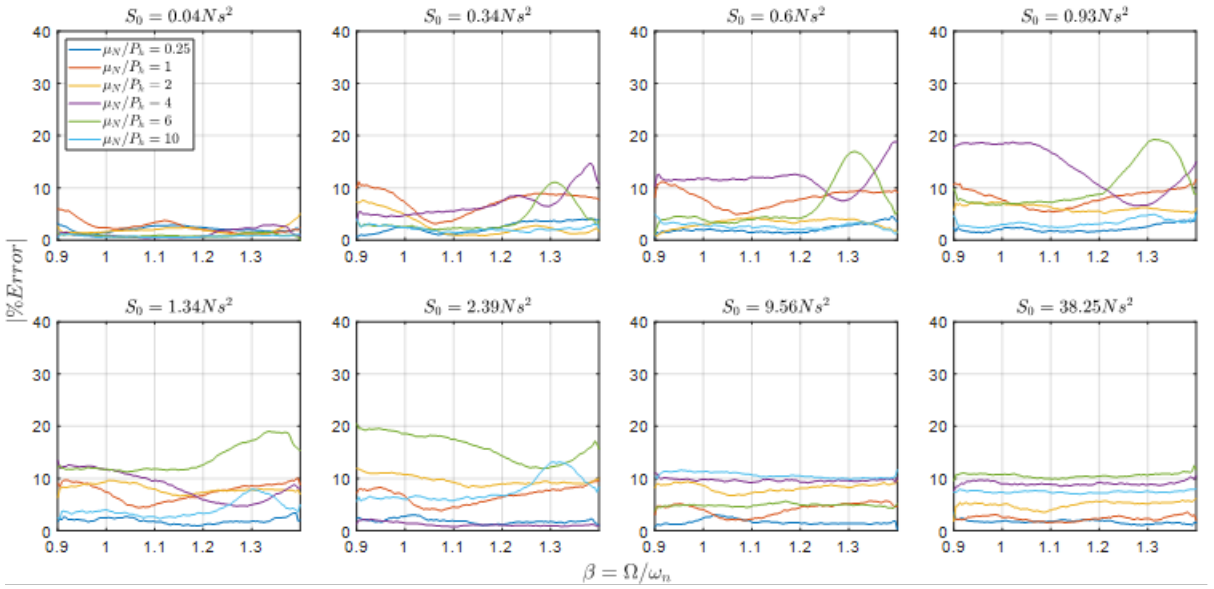

Fig. 9: Absolute percentage error of the proposed EL-TEE approach compared to benchmark time domain simulations for a range of random excitation amplitudes and contact forces.

$$\int_0^T E[\dot{v}_i f_{nl,j}]\,dt = \sum_k \sum_q 2\Big(k_{s,q} V_{y,q} V_{h,i}\Big(\sin(\Omega t_{3,q} + \phi_i) - \sin(\Omega t_{2,q} + \phi_i)\Big)\Big)$$
$$2\Big(k_{s,q}\Big(E[\dot{v}_{s,k} v_{r,k}] - E[\dot{v}_{r,i} v_{r,k}]\Big)\Big(t_{2,q} - t_{1,q}\Big) + k_{s,q}\Big(b_{i,j}(t_{1,q}, t_{2,q}) - b_{i,k}(t_{2,q}, t_{1,q})\Big)$$
$$+k_{s,q}(V_{y,q} - V_{max}) V_{h,i}\Big(\sin(\Omega t_{2,q} + \phi_i) - \sin(\Omega t_{1,q} + \phi_i)\Big)\Big) \quad (31)$$

Here $k_{s,q}$ and $V_{y,q}$ refer to the spring stiffness and slip displacement of the q^{th}Jenkins element in the Iwan element. Similarly, $t_{1,q}$, $t_{2,q}$ and $t_{3,q}$ refer to the transition times between branches of the nonlinearity for the q^{th} Jenkins element. These are calculated by applying Eq. (29) separately for each Jenkins element, where the auxiliary harmonic depends on the relative displacement across the Iwan element. As previously, subscripts i and j refer to degrees of freedom. $V_{h,i}$ and ϕ_i are the amplitude and phase of harmonic response at degree of freedom i, and $v_{r,i}$ is the random response component at degree of freedom i. Figure 10 is included to clarify the meaning of various subscripts.

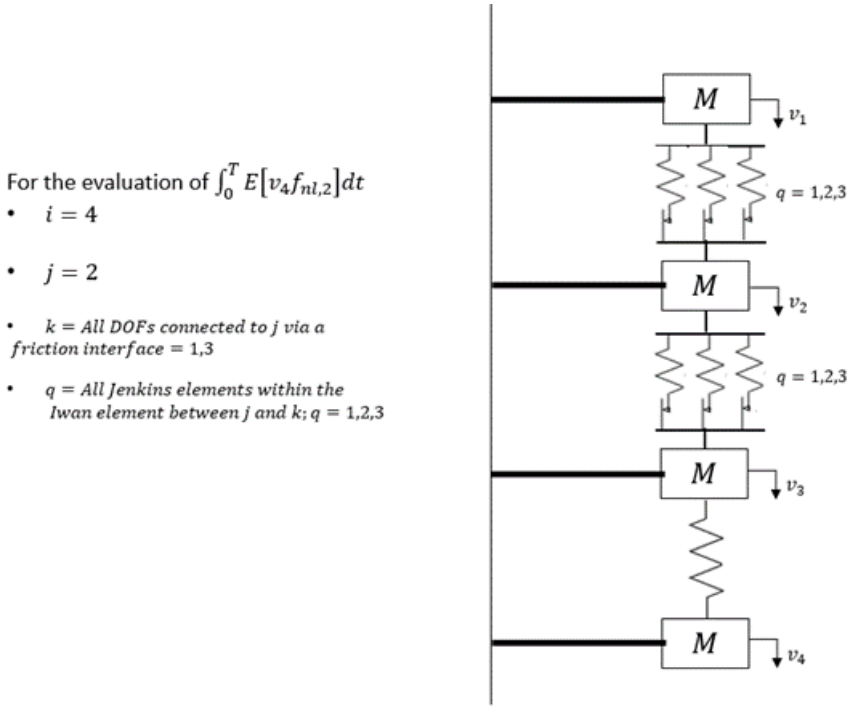

Fig. 10: An example system, illustrating the assignment of the various subscripts in the calculation of $\int_0^T E[v_i f_{nl,j}]\,dt$, for the example case where $i = 4$ and $j = 2$.

Figure 11 shows the test system used in this section to illustrate application of the method described above to a more complicated friction model. Two substructures are coupled via a frictional interface that is modelled by an Iwan element composed of three parallel Jenkins elements. Each substructure consists of a pair of masses on springs. Full details of the system are given in Table 1.

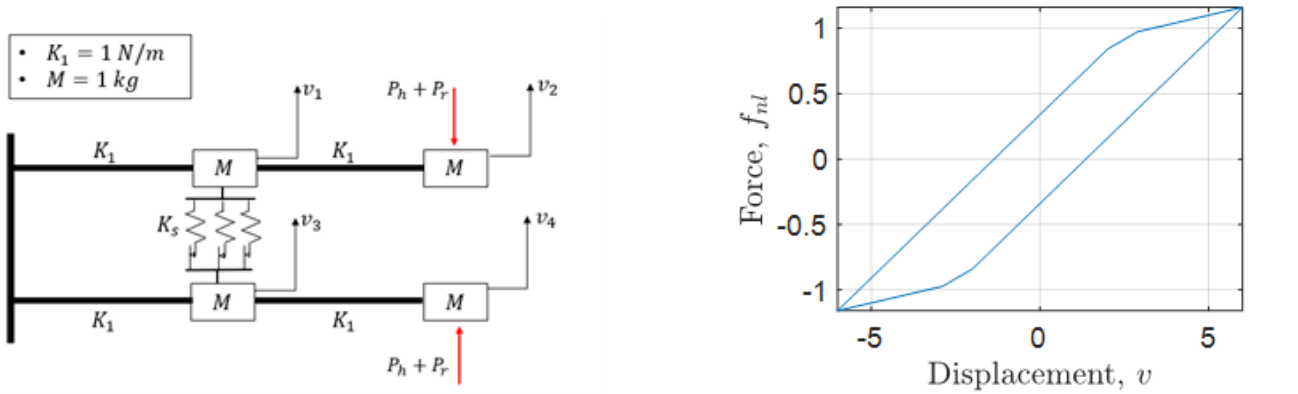

Fig. 11: (a) Multi-degree of freedom system with friction interface modelled by a parallel-series Iwan element and (b) example friction hysteresis loop.

Table 1: Parameters of the example system used in the analyses presented in Figure 13 to Figure 16.

	Example System 1 Figure 13, 15			Example System 2 Figure 14, 16		
	Element 1	Element 2	Element 3	Element 1	Element 2	Element 3
k_s	$0.1N/m$	$0.09N/m$	$0.06N/m$	$0.1N/m$	$0.09N/m$	$0.06N/m$
μ_N/P_h	0.4	0.4	0.4	1	1	1

The degrees of freedom indicated in Figure 11 are subjected to unit amplitude harmonic excitation ($P_h = 1N$) and uncorrelated white noise with a spectral density $S_0 = 810^{-5}N^2s$ and then $S_0 = 0.032N^2s$. Example excitation time histories for each of these scenarios are shown in Figure 12 in order to illustrate the nature of the excitation in the two cases. It can be appreciated qualitatively that in the first case the harmonic loading component is dominant, while in the second the random component is much greater.

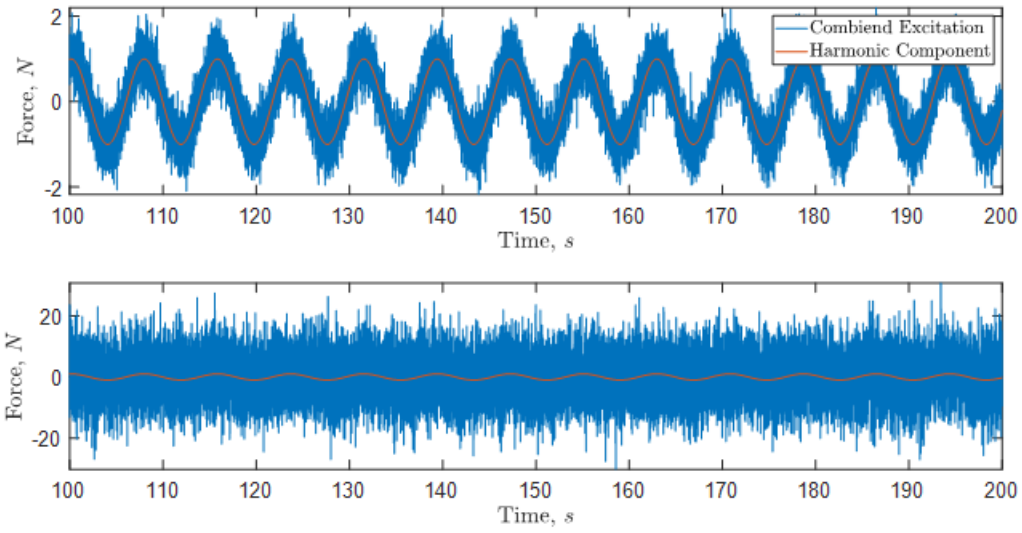

Fig. 12: Example excitation time histories for combined excitation with unit amplitude harmonic excitation with frequency $0.8s^{-1}$ and random white noise with $S_0 = 810^{-5}N^2s$ (corresponding to results presented in Figure 13 and Figure 14) and $S_0 = 0.032N^2s$ (corresponding to Figure 15 and Figure 16).

Figure 13 and Figure 14 compare the RMS displacement response of this system obtained using the EL-TEE approach, with the nonlinearity represented using the auxiliary harmonic, and time integration for two different values of the contact force at the point of slip, $\mu_N/P_h = 0.4N$ and $\mu_N/P_h = 1N$. In both cases the spectral density of the random excitation component is $810^{-5}N^2s$, with load time histories broadly similar to the example in the top subfigure in Figure 12. It can be appreciated that the proposed approach is capable of reproducing the results obtained from time integration, with almost identical values of RMS displacement obtained from both approaches. As shown in Table 2, the computational effort required to do this is much less for the EL-TEE, which offers a two orders of magnitude improvement on time integration.

Figure 15 and Figure 16 present similar results, except here the random excitation component has a spectral density of $0.032N^2s$, meaning excitation time histories are generally similar to the example in the lower subfigure in Figure 12. In this case, the random excitation component is substantial, however the proposed calculation approach employing the auxiliary harmonic is still capable of matching the results from time integration. Again, as shown in Table 2, the computational time required to do so is greatly reduced.

The influence of the number of Jenkins elements included in the Iwan element on calculation time is examined in Figure 17. This shows the response of similar analyses to the one presented in Figure 15 ($S_0 = 0.032N^2s$) for three systems with one ($K_s = 0.25N/m$, $\mu_N/P_h = 1.2$), three (Example System 1, detailed in Table 1) and six ($K_s = \{0.09, 0.06, 0.04, 0.03, 0.02, 0.01\}$, $\mu_N/P_h = \{0.4, 0.4, 0.1, 0.1, 0.1, 0.1\}$), Jenkins elements respectively. From Figure 17 it can be appreciated that the three systems exhibit broadly similar response. It can also be seen here that computational time does not increase with the number of Jenkins elements; in fact, counterintuitively, in the

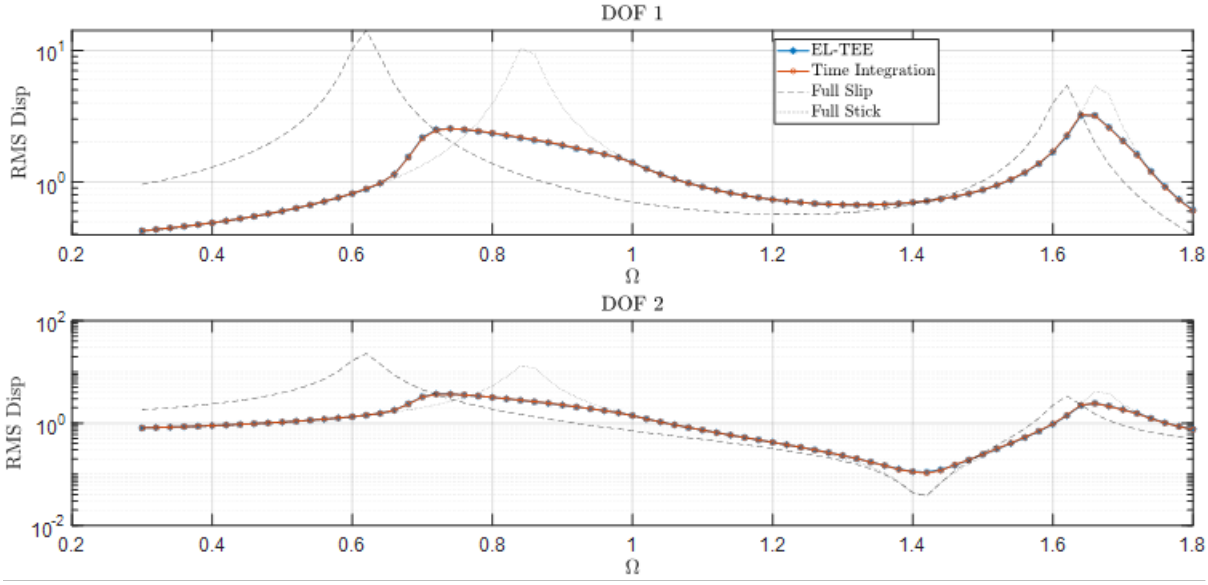

Fig. 13: Comparison of RMS displacement response calculated using the proposed EL-TEE approach and time integration for a MDOF system including a parallel-series Iwan element to combined harmonic and random excitation ($S_0 = 810^{-5} N^2 s$) across a range of harmonic excitation frequencies for Example System 1.

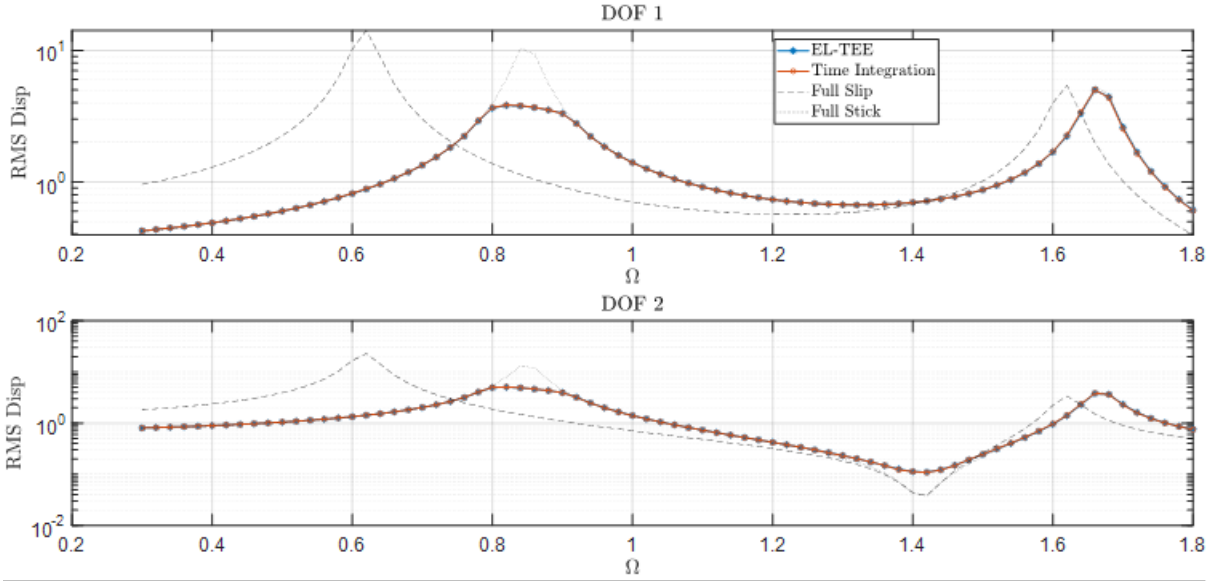

Fig. 14: Comparison of RMS displacement response calculated using the proposed EL-TEE approach and time integration for a MDOF system including a parallel-series Iwan element to combined harmonic and random excitation ($S_0 = 810^{-5} N^2 s$) across a range of harmonic excitation frequencies for Example System 2.

example case presented it actually decreases. This is because, in the particular example case examined, at certain frequencies a greater number of iterations are required to achieve convergence in the solution to the system of nonlinear equations for higher μ_N / P_h values. The number of iterations required for convergence depends strongly on the particular scenario under consideration, so no general conclusions about the relationship between number of Jenkins elements and computational speed should be drawn from Figure 17. However, it can be concluded that the increase in computational time compared to the SDOF case presented in Figure 7 is attributable to the increase in the number of degrees of freedom, as opposed to increasing the number of Jenkins elements. Similarly, the differences between computational times reported in Table 2 can be attributed to the number of iterations required in the solution to the system of nonlinear equations. Finally, when considering computational time, it should be noted that it may be possible to further optimize the solution algorithm for the system of nonlinear equations and thereby further reduce

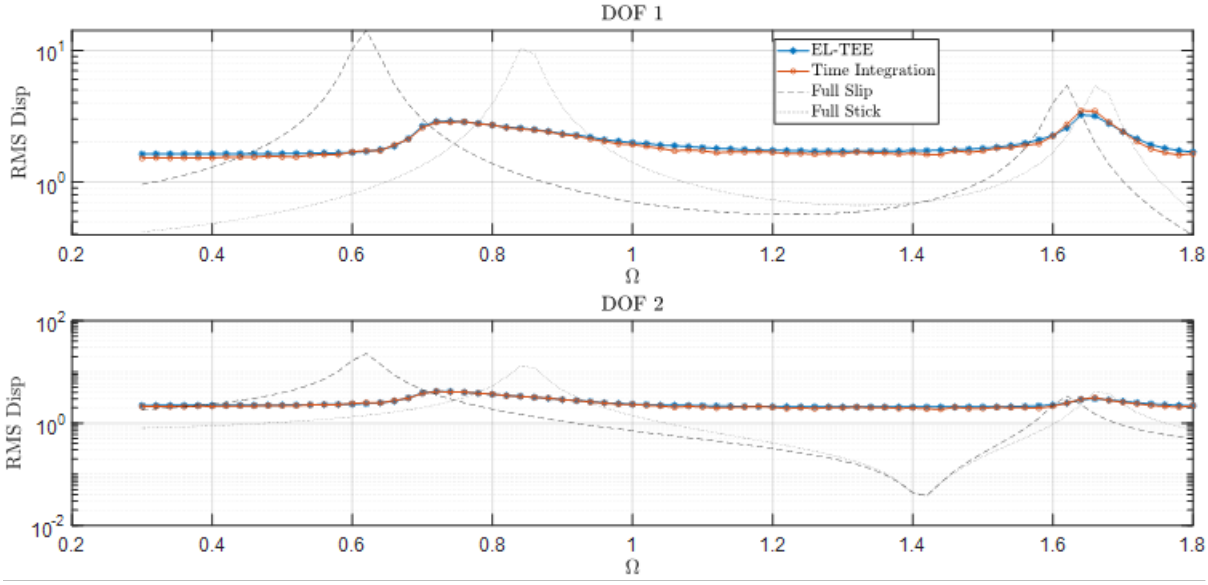

Fig. 15: Comparison of RMS displacement response calculated using the proposed EL-TEE approach and time integration for a MDOF system including a parallel-series Iwan element to combined harmonic and random excitation ($S_0 = 0.032N^2s$) across a range of harmonic excitation frequencies for Example System 1.

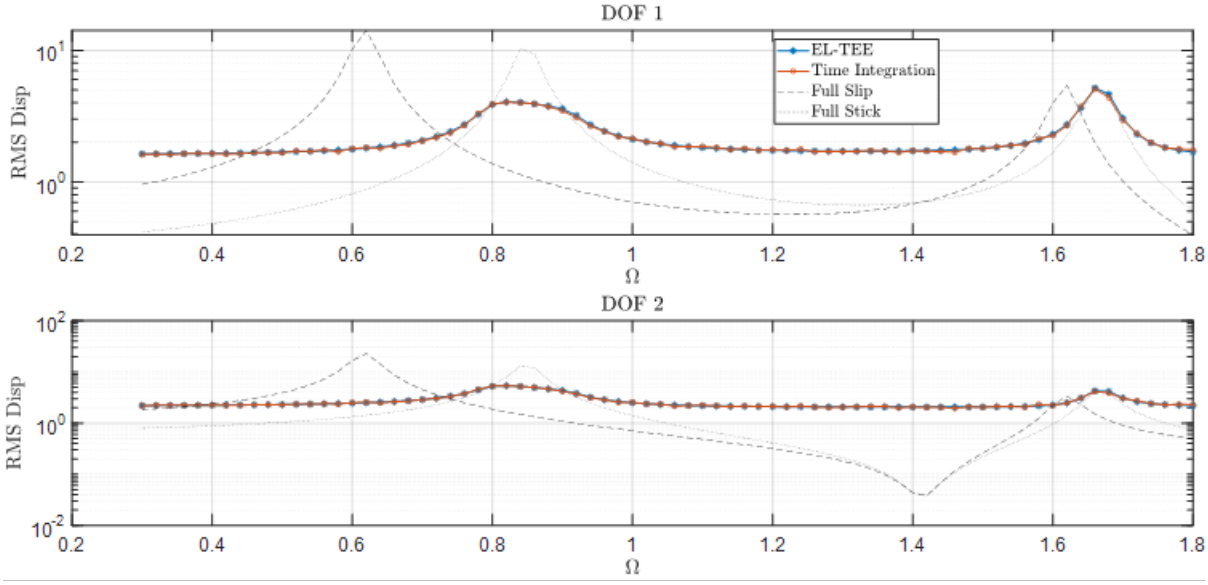

Fig. 16: Comparison of RMS displacement response calculated using the proposed EL-TEE approach and time integration for a MDOF system including a parallel-series Iwan element to combined harmonic and random excitation ($S_0 = 0.032N^2s$) across a range of harmonic excitation frequencies for Example System 2.

the computational expense, but this is beyond the scope of the work presented here.

Figure 18 demonstrates the effectiveness of the auxiliary harmonic approach for the case where $\mu_N/P_h = 0.4$ and $S_0 = 0.032N^2s$, i.e. the scenario shown in Figure 15, for the particular loading case where the harmonic excitation frequency, Ω, equals $0.8s^{-1}$. Comparing the hysteresis loops in Figure 18(a), it can be appreciated visually that the auxiliary harmonic approach allows the behaviour of the Iwan element to be approximated effectively. This can be quantified by comparing the cumulative energy dissipation calculated from time integration and from the auxiliary harmonic approach, as shown in Figure 18(b). As with the Jenkins element previously, it can be seen that these two values are very similar. Specifically the average energy dissipated over one harmonic loading cycle calculated from time integration is equal to $19.47Nm$ per cycle, while the equivalent value from the auxiliary harmonic approach is $19.83Nm$ per cycle. Again, this illustrates the success of the auxiliary harmonic approach in quantifying dissipative

Table 2: Time (in seconds) Required for EL-TEE and Time Integration.

Case	EL-TEE	Newmark-Beta
$\mu_N/P_h = 0.4$; Figure 13	6.68	340.84
$\mu_N/P_h = 1$; Figure 14	4.27	298.50
$\mu_N/P_h = 0.4$; Figure 15	2.77	338.98
$\mu_N/P_h = 1$; Figure 16	4.22	312.54

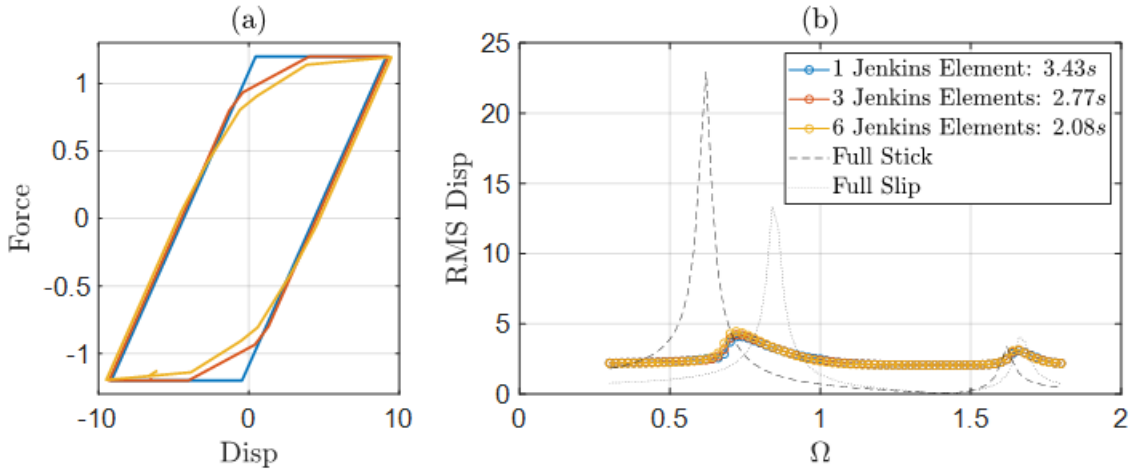

Fig. 17: Comparison of response of systems with Iwan elements composed of different numbers of Jenkins elements: (a) auxiliary harmonic hysteresis loops for the three systems for $\Omega = 0.8s^{-1}$ and (b) variation in RMS displacement at DOF 2 with harmonic excitation frequency, showing computational time.

behaviour under combined excitation, whilst maintaining the ability to analyse the nonlinearity analytically.

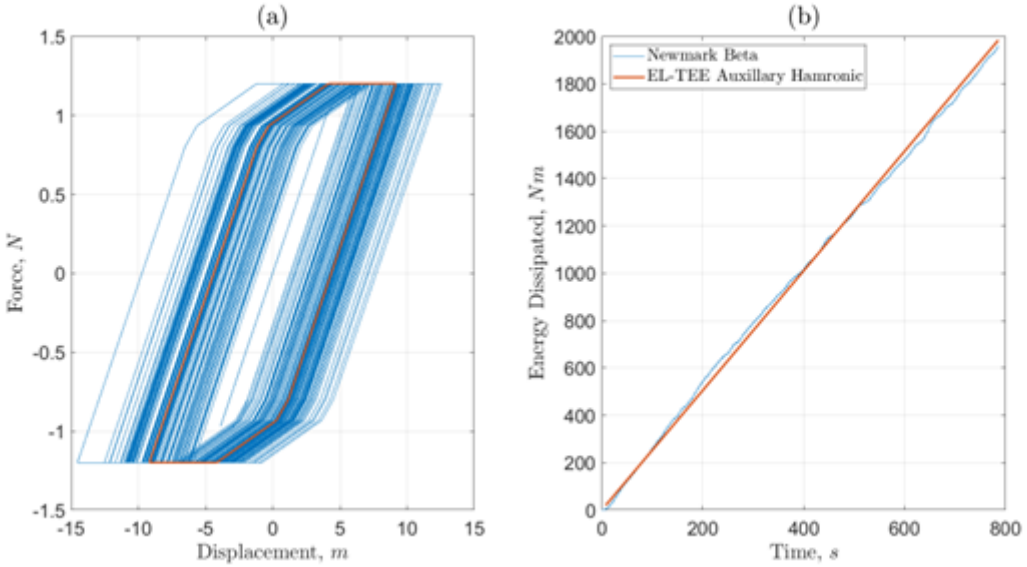

Fig. 18: Performance of the auxiliary harmonic approach for a parallel-series Iwan element: (a) Comparison of hysteresis loops from time integration and the auxiliary harmonic approach and (b) comparison of energy dissipated calculated from time integration and using the auxiliary harmonic.

5 Conclusion

This paper presents an efficient method for dynamic analysis of dry friction interfaces subjected to combined harmonic and random excitation. The proposed calculation approach is termed an Equivalent Linearization Time and Ensemble Expectation (EL-TEE) method, as it is based on linearizing over time and across the ensemble of random responses. Dry friction nonlinearity can be represented by the Jenkins element, or multiple Jenkins elements in parallel, termed the parallel-series Iwan element. In order to apply the proposed calculation approach to this representation of dry friction, a so-called auxiliary harmonic representation of the response is used to define the hysteresis loop. This allows analytical expressions for the nonlinear force to be obtained within the linearization process. The proposed method was compared to results of time integration for a number of example systems. It was demonstrated that the method was capable of faithfully reproducing the results of the time integration at a much reduced computational cost. Therefore, it is concluded the EL-TEE approach using the auxiliary harmonic representation of hysteresis is an effective and efficient way to analyse the type of discontinuous nonlinearities encountered in dry friction.

Appendix

A Evaluation of Integrals in Eq. (19)

Consider the linearization described by Eq. (19.c):

$$\int_0^T E\left[\begin{Bmatrix}\mathbf{v}\\ \dot{\mathbf{v}}\end{Bmatrix}\mathbf{f_{nl}}^T\right]dt = \left[\int_0^T E\begin{bmatrix}\mathbf{v}\mathbf{v}^\mathbf{T} & \dot{\mathbf{v}}\mathbf{v}^T\\ \mathbf{v}\dot{\mathbf{v}}^T & \dot{\mathbf{v}}\dot{\mathbf{v}}^T\end{bmatrix}dt\right]\begin{Bmatrix}\mathbf{K^e}^T\\ \mathbf{C^e}^T\end{Bmatrix} \tag{A.1}$$

Expanding:

$$\begin{matrix}\int_0^T E[\mathbf{v}\mathbf{f}_\mathbf{nl}^\mathbf{T}]\,dt\\ \int_0^T E[\dot{\mathbf{v}}\mathbf{f}_\mathbf{nl}^\mathbf{T}]\,dt\end{matrix} = \begin{matrix}\mathbf{K^e}\int_0^T E[\mathbf{v}\mathbf{v}^\mathbf{T}]\,dt\\ \mathbf{K^e}\int_0^T E[\dot{\mathbf{v}}\mathbf{v}^\mathbf{T}]\,dt\end{matrix} + \begin{matrix}\mathbf{C^e}\int_0^T E[\mathbf{v}\dot{\mathbf{v}}^\mathbf{T}]\,dt\\ \mathbf{C^e}\int_0^T E[\dot{\mathbf{v}}\dot{\mathbf{v}}^\mathbf{T}]\,dt\end{matrix} \tag{A.2}$$

Thus, six integrals need to be evaluated; $\int_0^T E[\mathbf{v}\mathbf{f}_\mathbf{nl}^\mathbf{T}]\,dt$, $\int_0^T E[\dot{\mathbf{v}}\mathbf{f}_\mathbf{nl}^\mathbf{T}]$, $\int_0^T E[\mathbf{v}\mathbf{v}^\mathbf{T}]\,dt$, $\int_0^T E[\dot{\mathbf{v}}\mathbf{v}^\mathbf{T}]\,dt$, $\int_0^T E[\mathbf{v}\dot{\mathbf{v}}^\mathbf{T}]\,dt$ and $\int_0^T E[\dot{\mathbf{v}}\dot{\mathbf{v}}^\mathbf{T}]\,dt$.

Firstly considering $\int_0^T E[\mathbf{v}\mathbf{v}^\mathbf{T}]\,dt$, which in index notation this can be expressed as:

$$\int_0^T E[\mathbf{v}\mathbf{v}^\mathbf{T}]\,dt = \int_0^T E[v_i v_j]\,dt \tag{A.3}$$

Noting that v_i is a combination of harmonic and random components:

$$v_i = v_{r,i} + v_{h,i} \tag{A.4}$$

Separating v_j into harmonic and random components similarly means:

$$\int_0^T E[v_i v_j]\,dt = \int_0^T E\Big[(v_{r,i} + v_{h,i})(v_{r,j} + v_{h,j})\Big]\,dt \tag{A.5}$$

Expanding:

$$\int_0^T E[v_i v_j]\,dt = \int_0^T E\Big[v_{r,i}v_{r,j} + v_{h,i}v_{r,j} + v_{r,i}v_{h,j} + v_{h,i}v_{h,j}\Big]\,dt \tag{A.6}$$

Taking expectations and noting that the expected value of the random components is zero:

$$\int_0^T E[v_i v_j]\,dt = \int_0^T E[v_{r,i}v_{r,j}]\,dt + \int_0^T v_{h,i}v_{h,j}\,dt \tag{A.7}$$

Now, noting that the harmonic response can be written as:

$$v_{hi} = V_{h,i}\sin(\Omega t + \phi_i) \tag{A.8}$$

Substituting and evaluating the integrals gives:

$$\int_0^T E[v_i v_j]\,dt = \int_0^T E[v_{r,i}v_{r,j}]\,dt + \int_0^T V_{h,i}\sin(\Omega t+\phi_i)V_{h,j}\sin(\Omega t+\phi_j)\,dt \tag{A.9}$$

$$\int_0^T E[v_i v_j]\,dt = T\left(E[v_{r,i}v_{r,j}] + \frac{1}{2}V_{h,i}V_{h,j}\cos(\phi_i-\phi_j)\right) \tag{A.10}$$

A similar process can be followed for the other integrals on the right-hand side of Eq. (A.2):

$$\int_0^T E[v_i \dot{v}_j]\,dt = T\left(E[v_{r,i}\dot{v}_{r,j}] + \frac{1}{2}V_{h,i}V_{h,j}\Omega\sin(\phi_i-\phi_j)\right) \tag{A.11}$$

$$\int_0^T E[\dot{v}_i v_j]\,dt = T\left(E[\dot{v}_{r,i}v_{r,j}] + \frac{1}{2}V_{h,i}V_{h,j}\Omega\sin(\phi_i-\phi_j)\right) \tag{A.12}$$

$$\int_0^T E[\dot{v}_i \dot{v}_j]\,dt = T\left(E[\dot{v}_{r,i}\dot{v}_{r,j}] + \frac{1}{2}V_{h,i}V_{h,j}\Omega^2\cos(\phi_i-\phi_j)\right) \tag{A.13}$$

Next, consider the expressions on the left hand side of Equation Eq. (A.2).Firstly examining $\int_0^T E[\mathbf{vf_{nl}^T}]\,dt$, which in index notation is $\int_0^T E[v_i f_{nl,j}]\,dt$.

The nonlinearity is described by the piecewise linear expression in Eq. (21). Considering the portion corresponding to Eq. (21.a). The 'v' here is relative displacement between nodes j and k, where k refers any node connected to node j via a friction interface.

$$\int_{t_1}^{t_2} E[v_i f_{nl,j}]\,dt = \int_{t_1}^{t_2} E\left[v_i k_s\left(\left(v_j - v_k\right) + \left(V_y - V_{max}\right)\right)\right]\,dt \tag{A.14}$$

Eq. (A.14) reduces to the expression for a single degree of freedom system if v_k is set to zero. Expanding Eq. (A.14) gives:

$$\int_{t_1}^{t_2} E[v_i f_{nl,j}]\,dt = k_s\int_{t_1}^{t_2} E\left[\left(v_i v_j - v_i v_k\right) + v_i\left(V_y - V_{max}\right)\right]\,dt \tag{A.15}$$

$$\int_{t_1}^{t_2} E[v_i f_{nl,j}]\,dt = k_s\int_{t_1}^{t_2} E\left[v_i v_j\right]\,dt - k_s\int_{t_1}^{t_2} E\left[v_i v_k\right]\,dt + k_s\left(V_y - V_{max}\right)\int_{t_1}^{t_2} E\left[v_i\right]\,dt \tag{A.16}$$

Separating the response into harmonic and random parts and then taking expectations leaves:

$$\begin{aligned}\int_{t_1}^{t_2} E[v_i f_{nl,j}]\,dt = {} & k_s\int_{t_1}^{t_2} E\left[\left(v_{h,i}+v_{r,i}\right)\left(v_{h,j}+v_{r,j}\right)\right]\,dt \\ & -k_s\int_{t_1}^{t_2} E\left[\left(v_{h,i}+v_{r,i}\right)\left(v_{h,k}+v_{r,k}\right)\right]\,dt \\ & +k_s\left(V_y - V_{max}\right)\int_{t_1}^{t_2} E\left[\left(v_{h,i}+v_{r,i}\right)\right]\,dt\end{aligned} \tag{A.17}$$

$$\begin{aligned}\int_{t_1}^{t_2} E[v_i f_{nl,j}]\,dt = {} & k_s\int_{t_1}^{t_2} E\left[v_{r,i}v_{r,j}\right]\,dt + k_s\int_{t_1}^{t_2} v_{h,i}v_{h,j}\,dt \\ & -k_s\int_{t_1}^{t_2} E\left[v_{r,i}v_{r,k}\right]\,dt - k_s\int_{t_1}^{t_2} v_{h,i}v_{h,k}\,dt \\ & +k_s\left(V_y - V_{max}\right)\int_{t_1}^{t_2} v_{h,i}\,dt\end{aligned} \tag{A.18}$$

Introducing a function $a_{i,j}$ such that:

$$a_{i,j}(t_2,t_1) = \int_{t_1}^{t_2} v_{h,i}v_{h,j}\,dt \tag{A.19}$$

Means that the solution to the integral can be expanded as:

$$\begin{aligned}\int_{t_1}^{t_2} E[v_i f_{nl,j}]\,dt &= k_s E\left[v_{r,i}v_{r,j}\right]\left(t_2-t_1\right) + k_s a_{i,j}(t_2,t_1)\\ &\quad -k_s E\left[v_{r,i}v_{r,k}\right]\left(t_2-t_1\right) - k_s a_{i,k}(t_2,t_1)\\ &\quad +\frac{k_s V_{h,i}\left(V_y - V_{max}\right)}{\Omega}\Big(\cos\left(\Omega t_2+\phi_i\right)-\cos\left(\Omega t_1+\phi_i\right)\Big)\end{aligned} \tag{A.20}$$

Which can be simplified to:

$$\begin{aligned}\int_{t_1}^{t_2} E[v_i f_{nl,j}]\,dt &= k_s\left(E\left[v_{r,i}v_{r,j}\right]-E\left[v_{r,i}v_{r,k}\right]\right)\left(t_2-t_1\right) + k_s\left(a_{i,j}(t_2,t_1)-a_{i,k}(t_2,t_1)\right)\\ &\quad +\frac{k_s V_{h,i}\left(V_y - V_{max}\right)}{\Omega}\Big(\cos\left(\Omega t_2+\phi_i\right)-\cos\left(\Omega t_1+\phi_i\right)\Big)\end{aligned} \tag{A.21}$$

If it is assumed that the transition between branches is periodic, it can be shown that:

$$t_3 = t_1 + \frac{T}{2} = t_1 + \frac{\pi}{\Omega} \tag{A.22}$$

$$t_4 = t_2 + \frac{T}{2} = t_2 + \frac{\pi}{\Omega} \tag{A.23}$$

Using this assumption, the integral corresponding to the branch of the nonlinearity described by Eq. (21.c) can also be shown to equal Eq. (A.22).

Now considering the part of the piecewise nonlinearity given by Eq. (21.b).

$$f_n l = k_s V_y \tag{A.24}$$

$$\int_{t_2}^{t_3} E[v_i f_{nl,j}]\,dt = \int_{t_2}^{t_3} E[v_i k_s V_y]\,dt \tag{A.25}$$

Separating response into random and harmonic components gives:

$$\int_{t_2}^{t_3} E[v_i f_{nl,j}]\,dt = k_s V_y \int_{t_2}^{t_3} E\left[\left(v_{h,i}+v_{r,i}\right)\right]\,dt \tag{A.26}$$

Taking expectations and evaluating the integrals gives:

$$\int_{t_2}^{t_3} E[v_i f_{nl,j}]\,dt = k_s V_y \frac{V_{h,i}}{\Omega}\Big(\cos\left(\Omega t_3+\phi_i\right)-\cos\left(\Omega t_2+\phi_i\right)\Big) \tag{A.27}$$

As before, if it is assumed that the hysteresis loop is periodic, it can be shown that the integral corresponding to the portion of the nonlinearity represented by Eq. (22.d) is also given by:

$$\int_{t_4}^{t_1} E[v_i f_{nl,j}]\,dt = k_s V_y \frac{V_{h,i}}{\Omega}\Big(\cos\left(\Omega t_3+\phi_i\right)-\cos\left(\Omega t_2+\phi_i\right)\Big) \tag{A.28}$$

Thus, the complete integral $\int_0^T E[v_i f_{nl,j}]\,dt$ is given by:

$$\begin{aligned}\int_0^T E[v_i f_{nl,j}]\,dt &= 2\left(k_s V_y \frac{V_{h,i}}{\Omega}\Big(\cos(\Omega t_3+\phi_i)-\cos(\Omega t_2+\phi_i)\Big)\right)\\ +2\Bigg(&k_s\Big(E\left[v_{r,i}v_{r,j}\right]-E\left[v_{r,i}v_{r,k}\right]\Big)\Big(t_2-t_1\Big)+k_s\Big(a_{i,j}(t_2,t_1)-a_{i,k}(t_2,t_1)\Big)\\ &+\frac{k_s V_{h,i}\Big(V_y-V_{max}\Big)}{\Omega}\Big(\cos(\Omega t_2+\phi_i)-\cos(\Omega t_1+\phi_i)\Big)\Bigg)\end{aligned} \tag{A.29}$$

Eq. (A.29) represents the value of $\int_0^T E[v_i f_{nl,j}]\,dt$ if it assumed that only one friction interface is connected to degree of freedom j. However, for completeness, all friction interfaces connected to j should be considered. Thus the value of $\int_0^T E[v_i f_{nl,j}]\,dt$ is Eq. (A.29) summed across all k, where k refers to any degree of freedom connected to j via a friction interface, as illustrated in Figure 10:

$$\begin{aligned}\int_0^T E[v_i f_{nl,j}]\,dt &= \sum_k 2\left(k_s V_y \frac{V_{h,i}}{\Omega}\Big(\cos(\Omega t_3+\phi_i)-\cos(\Omega t_2+\phi_i)\Big)\right)\\ +2\Bigg(&k_s\Big(E\left[v_{r,i}v_{r,j}\right]-E\left[v_{r,i}v_{r,k}\right]\Big)\Big(t_2-t_1\Big)+k_s\Big(a_{i,j}(t_2,t_1)-a_{i,k}(t_2,t_1)\Big)\\ &+\frac{k_s V_{h,i}\Big(V_y-V_{max}\Big)}{\Omega}\Big(\cos(\Omega t_2+\phi_i)-\cos(\Omega t_1+\phi_i)\Big)\Bigg)\end{aligned} \tag{A.30}$$

The expression for $\int_0^T E[\dot{v}_i f_{nl,j}]\,dt$ can be evaluated in a similar manner. For brevity, this derivation is not reproduced in full. However, by following the same steps as above and noting that $\dot{v}_{h,i} = V_{h,i}\Omega\sin(\Omega t+\phi_i)$, it can be shown that:

$$\begin{aligned}\int_0^T E[\dot{v}_i f_{nl,j}]\,dt &= \sum_k 2\Big(k_s V_y V_{h,i}\Big(\sin(\Omega t_3+\phi_i)-\sin(\Omega t_2+\phi_i)\Big)\Big)\\ +2\Bigg(&k_s\Big(E[\dot{v}_{r,i}v_{r,j}]-E[\dot{v}_{r,i}v_{r,k}]\Big)\Big(t_2-t_1\Big)+k_s\Big(b_{i,j}(t_1,t_2)-b_{i,k}(t_2,t_1)\Big)\\ &+k_s V_{h,i}(V_y-V_{max})\Big(\sin(\Omega t_2+\phi_i)-\sin(\Omega t_1+\phi_i)\Big)\Bigg)\end{aligned} \tag{A.31}$$

Where $b_{i,j}$ a function such that:

$$b_{i,j}(t_2,t_1) = \int_{t_1}^{t_2} \dot{v}_{hi}\dot{v}_{h,j}\,dt \tag{A.32}$$

Authors' Contributions

John Hickey: Conceptualization, Methodology, Software, Investigation, Writing - Original Draft Tore Butlin: Conceptualization, Methodology, Writing - Review & Editing, Supervision, Project Administration

Acknowledgements

The authors wish to acknowledge funding from Mitsubishi Heavy Industry Ltd and helpful discussions with Dr Naoki Onozato and Prof Robin Langley.

References

[1] D. Wang, C. Xu, X. Fan, and Q. Wan. Reduced-order modeling approach for frictional stick-slip behaviors of joint interface. *Mechanical Systems and Signal Processing*, 103:131–138, 2018.

[2] C. Beards. Damping in structural joints. *The shock and vibration digest*, 24(7):3–7, 1992.

[3] D. Yang, Z.-R. Lu, J. Liu, and L. Wang. An alternate state-space algorithm for dynamic solution, sensitivity analysis and parameter identification of dry friction systems. *Journal of Sound and Vibration*, 544:117383, 2023.

[4] S. Bograd, P. Reuss, A. Schmidt, L. Gaul, and M. Mayer. Modeling the dynamics of mechanical joints. *Mechanical systems and signal processing*, 25(8):2801–2826, 2011.

[5] A. T. Mathis, N. N. Balaji, R. J. Kuether, A. R. Brink, M. R. Brake, et al. A review of damping models for structures with mechanical joints. *Applied Mechanics Reviews*, 72(4):040802, 2020.

[6] L. Gaul and R. Nitsche. The role of friction in mechanical joints. *Applied Mechanics Review*, 54(2):93–106, 2001.

[7] J. Liu, H. Ouyang, Z. Feng, Z. Cai, J. Mo, et al. Dynamic behaviour of a bolted joint subjected to torsional excitation. *Tribology International*, 140:105877, 2019.

[8] Y. Sun, J. Yuan, L. Pesaresi, and L. Salles. Nonlinear vibrational analysis for integrally bladed disk using frictional ring damper. In *Journal of Physics: Conference Series*, volume 1106, page 012026. IOP Publishing, 2018.

[9] G. Cheng and J. W. Zu. Dynamics of a dry friction oscillator under two-frequency excitations. *Journal of Sound and vibration*, 275(3-5):591–603, 2004.

[10] H. Zhu, W. Zhu, and W. Fan. Dynamic modeling, simulation and experiment of power transmission belt drives: A systematic review. *Journal of Sound and Vibration*, 491:115759, 2021.

[11] M. Claeys, J.-J. Sinou, J. Lambelin, and R. Todeschini. Experiments and numerical simulations of nonlinear vibration responses of an assembly with friction joints–application on a test structure named “harmony”. *Mechanical Systems and Signal Processing*, 70:1097–1116, 2016.

[12] K. Sanliturk and D. Ewins. Modelling two-dimensional friction contact and its application using harmonic balance method. *Journal of sound and vibration*, 193(2):511–523, 1996.

[13] J. Armand, L. Pesaresi, L. Salles, and C. Schwingshackl. A multiscale approach for nonlinear dynamic response predictions with fretting wear. *Journal of Engineering for Gas Turbines and Power*, 139(2):022505, 2017.

[14] L. Pesaresi, L. Salles, A. Jones, J. Green, and C. Schwingshackl. Modelling the nonlinear behaviour of an underplatform damper test rig for turbine applications. *Mechanical Systems and Signal Processing*, 85:662–679, 2017.

[15] G. Scarselli, E. Castorini, F. Panella, R. Nobile, and A. Maffezzoli. Structural behaviour modelling of bolted joints in composite laminates subjected to cyclic loading. *Aerospace Science and Technology*, 43:89–95, 2015.

[16] W. D. Iwan. A distributed-element model for hysteresis and its steady-state dynamic response. *Journal of Applied Mechanics*, 33(4):893–900, 1966.

[17] D. J. Segalman. A four-parameter iwan model for lap-type joints. *Journal of Applied Mechanics*, 72(5):752–760, 2005.

[18] M. Oldfield, H. Ouyang, and J. E. Mottershead. Simplified models of bolted joints under harmonic loading. *Computers & Structures*, 84(1-2):25–33, 2005.

[19] H. Ouyang, M. Oldfield, and J. Mottershead. Experimental and theoretical studies of a bolted joint excited by a torsional dynamic load. *International Journal of Mechanical Sciences*, 48(12):1447–1455, 2006.

[20] P.-P. Yuan, W.-X. Ren, and J. Zhang. Dynamic tests and model updating of nonlinear beam structures with bolted joints. *Mechanical Systems and Signal Processing*, 126:193–210, 2019.

[21] N. Jamia, H. Jalali, J. Taghipour, M. Friswell, and H. H. Khodaparast. An equivalent model of a nonlinear bolted flange joint. *Mechanical Systems and Signal Processing*, 153:107507, 2021.

[22] D. Yang, Z.-R. Lu, and L. Wang. Parameter identification of bolted joint models by trust-region constrained sensitivity approach. *Applied Mathematical Modelling*, 99:204–227, 2021.

[23] K. Zong, Z. Qin, and F. Chu. Modeling of frictional stick-slip of contact interfaces considering normal fractal contact. *Journal of Applied Mechanics*, 89(3):031003, 2022.

[24] Y. Li and Z. Hao. A six-parameter iwan model and its application. *Mechanical Systems and Signal Processing*, 68:354–365, 2016.

[25] M. Brake. A reduced iwan model that includes pinning for bolted joint mechanics. *Nonlinear Dynamics*, 87:1335–1349, 2017.

[26] D. Li, D. Botto, C. Xu, T. Liu, and M. Gola. A micro-slip friction modeling approach and its application in underplatform damper kinematics. *International Journal of Mechanical Sciences*, 161:105029, 2019.

[27] M. Brake. Contact modeling across scales: from materials to structural dynamics applications. *Journal of Structural Dynamics*, 1:49–135, 2021.

[28] J. Yuan, F. Scarpa, B. Titurus, G. Allegri, S. Patsias, et al. Novel frame model for mistuning analysis of bladed disk systems. *Journal of Vibration and Acoustics*, 139(3):031016, 2017.

[29] E. Hairer, S. P. Nørsett, and G. Wanner. *Solving Ordinary Differential Equations I: Nonstiff Problems*. Springer, Berlin Heidelberg, 3 edition, 2008.

[30] G. J. Stein, R. Zahoranskỳ, and P. Múčka. On dry friction modelling and simulation in kinematically excited oscillatory systems. *Journal of Sound and Vibration*, 311(1-2):74–96, 2008.

[31] H. Kashani. Analytical parametric study of bi-linear hysteretic model of dry friction under harmonic, impulse and random excitations. *Nonlinear Dynamics*, 89(1):267–279, 2017.

[32] R. Mickens. Comments on the method of harmonic balance. *Journal of Sound and Vibration*, 94(3):456–460, 1984.

[33] J. B. Roberts and P. D. Spanos. *Random vibration and statistical linearization*. Dover Publicaitons Inc., Mineola, New York, 2003.

[34] I. Elishakoff and S. H. Crandall. Sixty years of stochastic linearization technique. *Meccanica*, 52:299–305, 2017.

[35] K. Ellermann. On the determination of nonlinear response distributions for oscillators with combined harmonic and random excitation. *Nonlinear Dynamics*, 42:305–318, 2005.

[36] B. Megerle, T. S. Rice, I. McBean, and P. Ott. Numerical and experimental investigation of the aerodynamic excitation of a model low-pressure steam turbine stage operating under low volume flow. In *Turbo Expo: Power for Land, Sea, and Air*, volume 44724, pages 403–414. American Society of Mechanical Engineers, 2012.

[37] D. H. Hawes and R. S. Langley. Numerical methods for calculating the response of a deterministic and stochastically excited duffing oscillator. *Proceedings of the Institution of Mechanical Engineers, Part C: Journal of Mechanical Engineering Science*, 230(6):888–899, 2016.

[38] H.-w. Rong, W. Xu, and T. Fang. Principal response of duffing oscillator to combined deterministic and narrow-band random parametric excitation. *Journal of Sound and Vibration*, 210(4):483–515, 1998.

[39] W. Zhu and Y. Wu. First-passage time of duffing oscillator under combined harmonic and white-noise excitations. *Nonlinear Dynamics*, 32:291–305, 2003.

[40] R. Haiwu, X. Wei, M. Guang, and F. Tong. Response of a duffing oscillator to combined deterministic harmonic and random excitation. *Journal of Sound and Vibration*, 242(2):362–368, 2001.

[41] H.-T. Zhu and S.-S. Guo. Periodic response of a duffing oscillator under combined harmonic and random excitations. *Journal of Vibration and Acoustics*, 137(4):041015, 2015.

[42] N. Anh and N. Hieu. The duffing oscillator under combined periodic and random excitations. *Probabilistic Engineering Mechanics*, 30:27–36, 2012.

[43] C. Manohar and R. Iyengar. Entrainment in van der pol's oscillator in the presence of noise. *International journal of non-linear mechanics*, 26(5):679–686, 1991.

[44] N. Anh, V. Zakovorotny, and D. Hao. Response analysis of van der pol oscillator subjected to harmonic and random excitations. *Probabilistic Engineering Mechanics*, 37:51–59, 2014.

[45] P. D. Spanos, Y. Zhang, and F. Kong. Formulation of statistical linearization for mdof systems subject to combined periodic and stochastic excitations. *Journal of Applied Mechanics*, 86(10):101003, 2019.

[46] F. Kong and P. D. Spanos. Stochastic response of hysteresis system under combined periodic and stochastic excitation via the statistical linearization method. *Journal of Applied Mechanics*, 88(5):051008, 2021.

[47] S. Biswas and A. Chatterjee. A reduced-order model from high-dimensional frictional hysteresis. *Proceedings of the Royal Society A: Mathematical, Physical and Engineering Sciences*, 470(2166):20130817, 2014.

[48] J. Hickey, T. Butlin, R. Langley, and N. Onozato. A time and ensemble equivalent linearization method for nonlinear systems under combined harmonic and random excitation. *Proceedings of the Institution of Mechanical Engineers, Part C: Journal of Mechanical Engineering Science*, 238(9):3724–3745, 2024.

[49] N. M. Newmark. A method of computation for structural dynamics. *Journal of the engineering mechanics division*, 85(3): 67–94, 1959.